Petrogenesis and geodynamic setting of Ediacaran rocks from the Sirwa massif, Central Anti-Atlas of Morocco

Abdelhay Ben-Tami[1,2], Saïd Belkacim[1,6], Jamal El Kabouri[1], Bouchra Baidada[3], Joshua H.F.L. Davies[4], Morgann G. Perrot[5], Mohamed Bhilisse[2], Mohamed Assalmi[2], Mariam Ferraq[1,6], Mohamed Bouabdellah[7,8]

[1] Laboratoire de Géologie Appliquée et Géo-Environnement, Département de la Géologie, Faculté des Sciences, Université Ibn Zohr, B.P.8106, Agadir, Maroc.
[2] Zgounder Millennium Silver Mining, Aya Gold and Silver Group, Rue De L'epargne, Quartier Racine, Casablanca, Maroc.
[3] Higher school of Technology, Fkih Ben Salah, Beni Mellal, Morocco.
[4] Department of Earth and Atmosphere Sciences, University of Quebec in Montreal, Montreal, QC H3C 3P8, Canada.
[5] Department of Earth and Planetary Sciences, McGill University, Montreal, Quebec H3A 0E8, Canada.
[6] Mining and Environmental Research Institute, University of Quebec in Abitibi-Timiskaming, Rouyn-Noranda, QC J9X 5E4, Canada.
[7] Laboratoire des Gîtes Minéraux, Hydrogéologie et Environnement, Faculté des Sciences, Université Mohammed Premier, 60000, Oujda, Maroc.
[8] Geology and Sustainable Mining Institute, Mohammed VI Polytechnic University, Benguerir 43150, Morocco.

Correspondence to: Abdelhay Ben-Tami (abdelhaybentami@gmail.com)

Abstract

The geodynamic evolution of the post-Pan-African Anti-Atlas Orogeny (~650 Ma) remains debated, particularly regarding the basement beneath the Central Anti-Atlas and the geological processes leading to the formation of the Ediacaran Saghro Group (SG) and Ouarzazate Group (OG). New LA-ICP-MS U-Pb ages of 575 ± 3 Ma and 564 ± 2 Ma were obtained from two OG magmatic rocks. Detrital zircons from the SG yield a 2025 Ma maximum depositional age (MDA) and a prominent 2100 Ma peak, indicating exclusive recycling of Paleoproterozoic basement into the Ediacaran SG basin. Geochemically, two magmatic series are identified: (i) SG mafic rocks with a calc-alkaline, within-plate signature and negative Nb-Ta and Ti anomalies, consistent with a back-arc basin setting; and (ii) an OG felsic-intermediate, high-K calc-alkaline to shoshonitic series of post-collisional character. Isotope data (εNd_{620} = +3.2 to +4.6, TDM = 1.02–0.91 Ga for the SG; εNd_{570} = -0.8 to +1.1, TDM = 1.30–1.15 Ga for the OG) indicate that the SG formed from a near-pristine mantle source with limited crustal input, whereas the younger OG involved significant reworking of older, evolved continental crust.

These findings support a model in which early Ediacaran SG sediments and associated magmatic rocks were deposited in a back-arc basin. During this basin development, its shoulders were locally formed by the 2100 Ma Paleoproterozoic basement, supplying Paleoproterozoic zircons to the Saghro basin without interaction with Ediacaran sediments and corroborating the extension of the Eburnian basement north of the Anti-Atlas Major Fault (AAMF). The younger OG subsequently recorded a late Ediacaran post-collisional crustal collapse event, during which lithospheric delamination and potential slab break-off drove widespread crustal reworking and emplacement of a Silicic Large Igneous Province (SLIP).

Keywords

Anti-Atlas; Ediacaran; LA-ICP-MS U-Pb geochronology; Saghro Group (SG); Ouarzazate Group (OG); 2.1 Ga Paleoproterozoic crust

1 Introduction

The Anti-Atlas belt of Morocco, located along the northern margin of the West African Craton (WAC), bears witness to a long-lived geological evolution since the break-up of Rodinia (Hefferan et al., 2014; Gasquet et al., 2008; Thomas et al., 2002). Initial rifting at ca. 900–700 Ma is recorded by the 885 Ma Tonian mafic dikes. This rifting generated a passive margin along the WAC and eventually led to the development of Cryogenian oceanic lithosphere (Hefferan et al., 2014). This period is characterized by the deposition of the Lkest-Taghdout Group, a thick sequence of quartzites and carbonates (Alvaro et al., 2014b) (Fig. 1B). The subsequent evolution of the Anti-Atlas belt during the Ediacaran remains debated, despite major advances in understanding the multiple Neoproterozoic events that culminated in the final amalgamation of Gondwana (D'Lemos et al. 2006; Samson et al. 2004; Gasquet et al. 2008, 2005, 2004; Thomas et al. 2004, 2002; Ennih and Liégeois, 2008, 2001; Walsh et al. 2002). Based on paleogeographic reconstructions and lithostratigraphic correlations (Linnemann et al., 2014; Errami et al., 2021a; Walsh et al., 2012), the Anti-Atlas belt was close to the Cadomian subduction system. Whereas Gondwana amalgamation was driven by large-scale Pan-African collisions between major cratonic blocks, the northern margin of the WAC experienced a synchronous but distinct tectonic regime (Rojo-Pérez et al., 2024; Stern, 2024; Hefferan et al., 2014). During the Ediacaran, this margin lay proximal to the Cadomian accretionary system, a long-lived subduction-related orogen that developed along the Gondwanan periphery (Linnemann et al., 2014; Nance et al., 2008).

It remains debated whether the Anti-Atlas records the post-collisional stage of the Pan-African belt or instead reflects the development of a back-arc basin induced by the southward-dipping Cadomian subduction beneath the amalgamated WAC-Iriri/Tazigzaout arc complex at ca. 620 Ma (Errami et al., 2021a; Walsh et al., 2012; El Hadi et al., 2010; Abati et al., 2010). The nature of the basement north of the AAMF also remains unresolved (Ennih and Liégeois, 2008, 2001).

In the Zgounder Mine Region (ZGMR), a well-preserved section of Ediacaran sedimentation and magmatism, provides key insights into the final stages of Pan-African tectono-magmatic evolution along the northern margin of the WAC. Here, we present new whole-rock geochemical, and Sm-Nd isotopic data to decipher the petrogenesis of these rocks, explore magma sources, and assess their geodynamic significance in the Ediacaran evolution of the WAC. We also report new LA-ICP-MS U-Pb ages from magmatic and detrital zircons to constrain the lower Ediacaran magmatism and evaluate the provenance of the Saghro Group sedimentary units, thereby refining existing geodynamic models.

2 Geological background

The Anti-Atlas belt consist of a Proterozoic basement and a late Ediacaran to Paleozoic cover (Leblanc and Lancelot, 1980) (Fig. 1B). It records two major orogenic cycles: the Paleoproterozoic Eburnean and the Neoproterozoic Pan-African, classically separated by the AAMF (Fig. 1B). The Paleoproterozoic Eburnean Orogeny is preserved in the Western Anti-Atlas, where low- to high-grade metamorphic rocks are intruded by granitoids dated at ~2.2 Ga (Hefferan et al., 2014, and references therein; O'Connor et al., 2010; El Hadi et al., 2010; Gasquet et al., 2008, 2005; Thomas et al., 2002; Walsh et al., 2002; Aït Malek et al., 1998). The Central Anti-Atlas features the ophiolitic sequences and island-arc complexes of the Bou Azzer and Sirwa massifs (Admou et al., 2012; D'Lemos et al., 2006; Thomas et al., 2002, 2004). To the east, the Eastern Anti-Atlas comprises the Jbel Saghro and Ougnat massifs, composed exclusively of Neoproterozoic Pan-African units (Fig. 1B): an early Ediacaran SG basement of folded meta-sedimentary rocks metamorphosed under greenschist facies conditions, unconformably overlain by late Ediacaran OG volcanic and volcano-sedimentary successions (Ouabid and Garrido, 2023; Errami et al., 2021a; Yajioui et al., 2020; Michard et al., 2017; Blein et al., 2014; Álvaro et al., 2014, 2014b; Walsh et al., 2012; Abati et al., 2010; Errami et al., 2009; Gasquet et al., 2008; Liégeois et al., 2006; Thomas et al., 2002; Fekkak et al., 2001; Bajja, 2001; Ouguir et al., 1996).

This study focuses on the Ediacaran (630–539 Ma) of the Sirwa massif. Recent 1/50 000 scale mapping of the Douar Çour, Assarrag, Tachoukacht, Tamallakout, Sirwa, Taghdout, and Açdif (see Fig. 1C) subdivided the Sirwa massif into several groups (Thomas et al., 2000a; De Beer et al., 2000; Gresse et al., 2000). The oldest units belong to the Bleida Group, comprising schists and orthogneisses dated at 743 ± 14 Ma (Fig. 1C) (Thomas et al., 2002), overlain by the SG (Thomas et al., 2002): a thick deformed succession of calc-alkaline volcanic rocks, and sedimentary units metamorphosed under greenschist-facies conditions. The SG comprises six formations: Tittalt, Agchtim, Imghi, Tizoula, Azarwas, and Tafiat (Thomas et al., 2002), with a lower greywacke/turbidites-volcanic sequence and upper coarse-grained clastic formations. U-Pb detrital zircon dating indicates a maximum depositional age of ca. 610 Ma (Abati et al., 2010; Liégeois et al., 2006), with more recent ages of 607 ± 6 Ma and 604 ± 5 Ma (Errami et al., 2021a). Within the Sirwa inlier, depositional age of the SG is constrained by the Mzil granite dated at 614 ± 10 Ma (Thomas et al., 2002, 2004).

The Bou Salda Group, a volcano-sedimentary succession from 610 to 580 Ma (Gasquet et al., 2008), represents basin infills of grabens and pull-apart basins within the AAMF (Errami et al., 2021a; Gasquet et al., 2008; Thomas et al., 2002). The age of the Bou Salda Group is derived from the Tadmant and Tamriwine rhyolites, dated respectively at 606 ± 6 Ma and 605 ± 9 Ma (Thomas et al., 2002) (Fig. 1C, and Fig. 2). Pelleter et al. (2016), also dated the Tadmant rhyolite at 610 ± 7 Ma (Fig. 2). Nonetheless, Abati et al. (2010) report ca. 600 Ma detrital ages in the Bou Salda Group indicating a coeval volcanogenic input. The OG sequences (580–539 Ma; Blein et al., 2014b; Toummite et al., 2013; Thomas et al., 2002, 2004) of immature, coarse clastic sedimentary rocks (conglomerates, arkoses, reworked volcanic rocks), acid to intermediate volcaniclastic rocks (lapilli tuff, volcanic breccias, ignimbrites, etc.), and lavas (minor basalt, andesite and rhyolite) are associated with post-collisional high-K calc-alkaline to shoshonitic magmatism (Soulaimani et al., 2018). Throughout the Sirwa inlier, the OG is subdivided into four subgroups: Tiouin, Bouljama, Tafrant, and Achkoukchi (Fig. 1C) (Thomas et al., 2000a; Gresse et al., 2000; De Beer et al., 2000). Under an extensional regime, foreland basin successions of the Tata Group were deposited following the post-orogenic molasse volcaniclastic rocks of the OG (Thomas et al., 2002) (Fig. 1C).

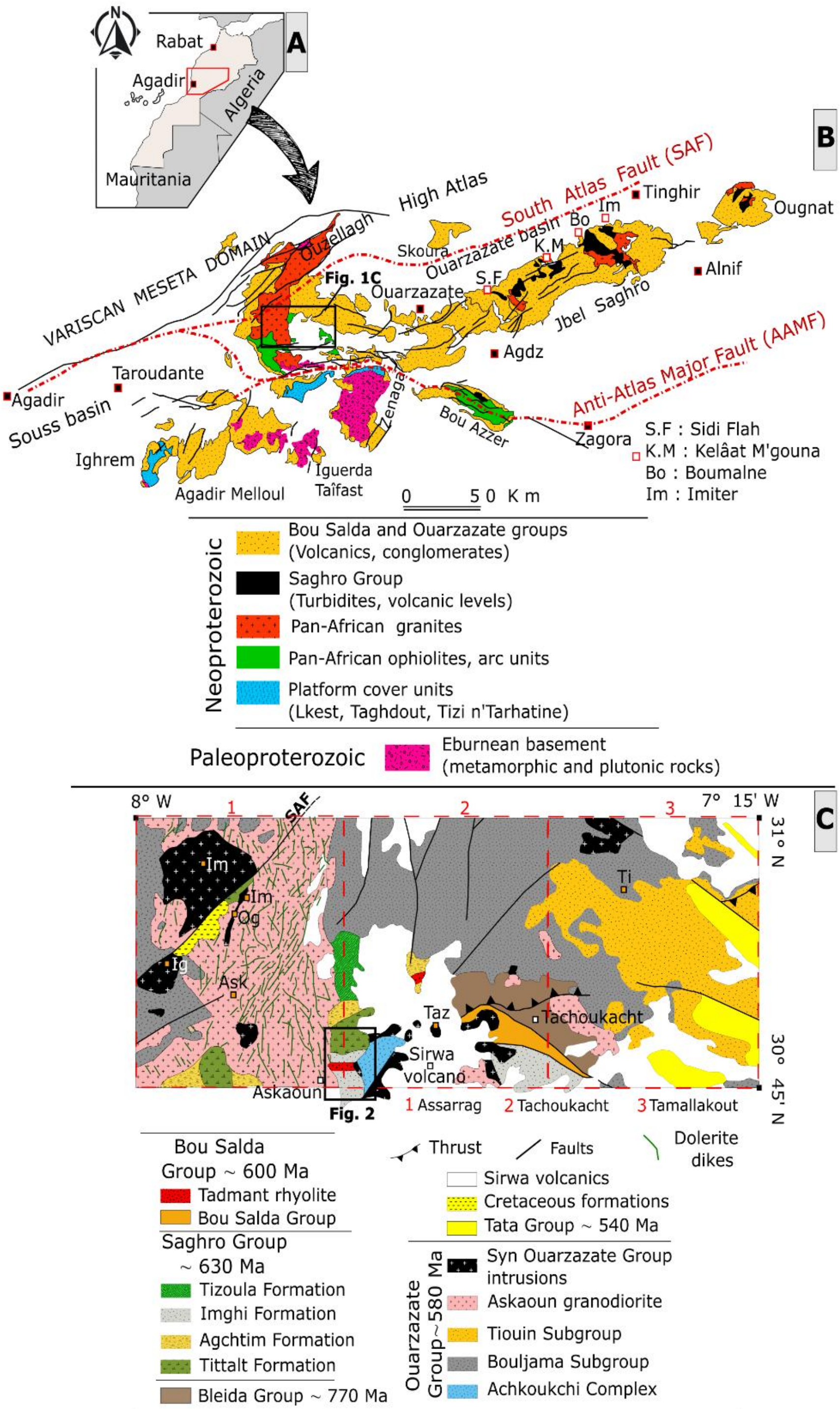

Figure 1. (A) Sketch map locating the Anti-Atlas belt in respect to Morocco (Saadi, 1985); (B): geological map of the Central and Eastern Anti-Atlas Proterozoic inliers (redrawn and modified after Michard et al. (2017); (C): Schematic representation of the

geology of the Sirwa massif (compiled and redrawn from Thomas et al. (2002); location of the ZGMR in Figure. 2. Abbreviations: Taz : Tazoult quartz-porphyry (559 ± 6 Ma); Im: Imourkhssen granite (562 ± 5 Ma); Ti: Tikhfist rhyolite (571 ± 8 Ma); Ask: Askaoun granodiorite (575 ± 8 Ma); Ig: Ighrem granite; Og: Ougougane granite; and SAF: South Atlas Fault. U-Pb ages are from Thomas et al. (2002).

2.1 Field characteristics and sample distribution

The study area (Fig. 2), hereafter the ZGMR "Zgounder Mine Region" corresponds to the vicinity of the Zgounder Ag-Hg deposit, located 265 km east of Agadir, and 220 km west of Ouarzazate, along the southern flank of the Ouzellagh-Sirwa Salient in the Central Anti-Atlas Mountains (Ben-Tami et al., 2024). Detailed geological mapping across the ZGMR established the primary lithostratigraphic relationships (Fig. 2). The Ediacaran of the ZGMR (630–539 Ma) comprises: (i) the SG sedimentary successions and coeval magmatic rocks deposited 630 to 600 Ma (Errami et al., 2021a; Abati et al., 2010); and (ii) large felsic plutons, subvolcanic formations, and coeval pyroclastic rocks, referred to as the OG (600–539 Ma; Thomas et al., 2002).

The oldest rocks in the study area belong to the SG: the northern, E-W-striking Tittalt Formation and the southern Imghi Formation (Fig. 2). The lowermost Tittalt Formation consists of basaltic and andesitic volcanic rocks associated with a gabbroic intrusion, bounded to the south by the Imghi Formation. The Imghi Formation features poorly graded, thick-bedded greywacke of stacked fine- to very fine-grained sandstone beds, and greyish-green, well-bedded, graded turbidites striking east and dipping steeply south at 70° (Fig. 2). Felsic magmatism is represented by the E-W-trending Tadmant rhyolite (Bou Salda Group; Thomas et al., 2002), forming the core of the area between the western Askaoun granodiorite and the eastern OG sequences (Fig. 2). Other subvolcanic activities include the E-W-trending rhyolitic dikes and plugs of the Assarrag suite (Thomas et al., 2002). Post-SG, post-Bou Salda magmatism includes the Askaoun granodiorite, intruding the western Imghi Formation, and the syn- to late-Ouarzazate Bou-Tazart granite (Amassine Suite; Thomas et al., 2002). To the east, the sub-horizontal volcano-sedimentary packages of the OG consist of laminated ignimbrites, ignimbritic rhyolites, andesites, and lapilli tuffs containing volcanic glass lenses. Associated mafic activity is recorded by an intermittent, fault-offset dolerite/diabase sill-like body (~25 m surface width),parallel to the rhyolite-sediment contact (Fig. 2).

A total of 32 samples were collected from the Saghro and Ouarzazate groups for petrographic and geochemical analysis. For each sample, lithostratigraphic position, sample type, drill core name and depth, short description and analytical methods applied are reported in Supplementary Table 1. Three samples were selected for U-Pb geochronology: (i): a laminated, light-pink to brownish rhyolitic dike crosscutting the Tittalt Formation (Zg-106; 46 m long, 4–5 m thick; Fig. 2); (ii): a fine- to medium-grained, light grey granite (Zg-119) from drill hole ZG-20-21 at 555.30–568.50 m intruding the Imghi Formation; and (iii): a fine- to medium-grained greenish SG sandstone collected near the Zgounder Mine main entrance for detrital zircon analysis (Zg-132; Fig. 2) (Supplementary Table 2).

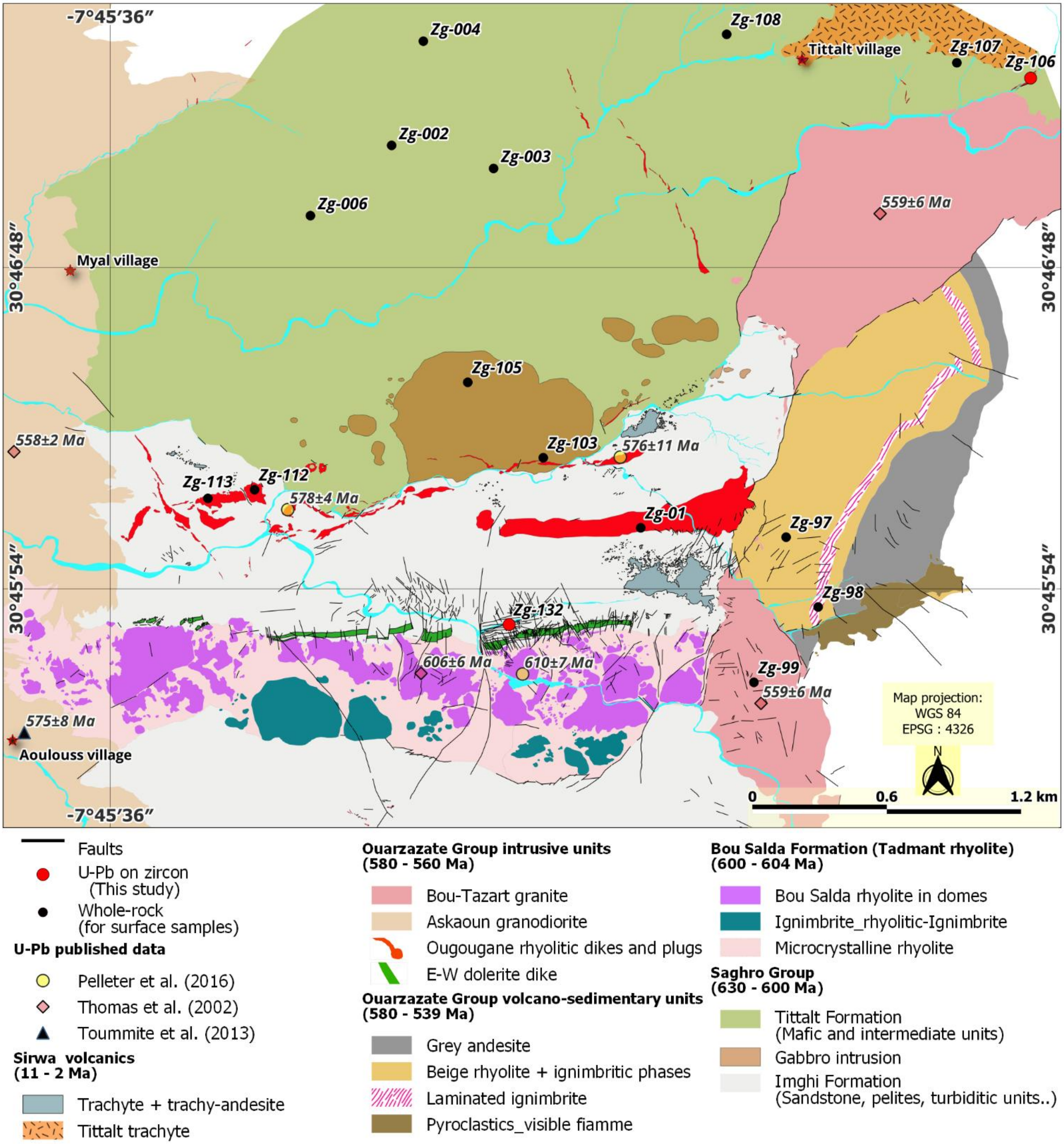

Figure 2. Detailed geological map of the ZGMR (this study). Locations of surface samples are indicated on the map. Underground samples (Mine levels, drill holes) including the dated Zg-119 are not represented on the map.

3 Data and methodology

3.1 U-Pb zircon geochronology

Sample preparation for U-Pb zircon geochronology involved crushing, sieving to 50–250 µm, and weighing (1.4 kg for Zg-106; 1.5 kg for Zg-119; 2.3 kg for Zg-132) at the Département de Géologie, Faculté des Sciences, Université Ibn Zohr, Maroc. Samples were then shipped to the Geotop Research Center, Université du Québec à Montréal (UQAM), Canada. Analytical parameters are detailed in Supplementary Data 1, following Horstwood et al. (2016). Ages of intrusive rocks are reported as weighted mean $^{206}Pb/^{238}U$ dates, calculated using the "exclude outliers" function in Isoplot R, and detrital zircon data as concordia dates. LA-ICP-MS U-Pb data are given in Supplementary Table 2.

3.2 Whole-rock geochemistry and Sm-Nd isotopes

Fresh rock samples were collected for whole-rock geochemistry and Sm-Nd isotopes from outcrops (surface and underground), as well in various diamond drill holes from the ZGMR. Crushing and powdering were performed at the facilities of the Zgounder Millennium Silver Mining Company (ZMSM). Further analytical procedures are detailed in Supplementary Data 1, and results are shown in Supplementary Table 3.

4 Results

4.1 Petrography

4.1.1 The SG magmatic rocks

- The SG is mainly represented by fine to medium-grained, dolerite to basaltic-andesite samples. A medium- to coarse-grained, equigranular, dark green gabbroic facies is also present, showing heavily altered pyroxenes and amphiboles (Fig. 3a). The SG mafic volcanics contain fine-grained plagioclase and clinopyroxene phenocrysts dispersed in the groundmass. The dolerite sample (Fig. 3b) has an intergranular texture, with primary Fe-Ti oxides, clinopyroxene aggregates, and lath-shaped plagioclase. Sample Zg-108 is andesitic in composition (Fig. 3c), with an ophitic texture. Basalt and basaltic-andesite samples show a microlitic to microlitic-porphyritic texture (Fig. 3d).

4.1.2 The SG sedimentary sample

- The dated sandstone sample (Zg-132) displays alternating patterns with distinct, well-defined, millimeter-scale laminations controlled by compositional variations. Darker bands are enriched in chlorite, whereas lighter laminae are mainly composed of quartz and muscovite (Fig. 3e).

4.1.3 The OG magmatic rocks

- Rhyolite samples show a microcrystalline, locally glassy texture. Primary mineral assemblages, composed of quartz megacrysts and K-feldspar altered to albite, are embedded in a devitrified matrix. Secondary alteration minerals include sericite and albite, with some local carbonate veinlets (Fig. 3f). Dolerite samples (Zg-13, Zg-15; Fig. 3g) are fine-grained, exhibiting an intergranular texture. They show equant opaque grains enclosed within primary minerals (plagioclase, pyroxene); plagioclase crystals, locally transformed to albite, are moderately sericitized and locally altered to epidote. A dolerite sample (Zg-14) collected next to the mineralized zone has an intergranular texture in which laths of black, oxidized plagioclase are included in pyroxene crystals (Fig. 3h). Clinopyroxene is mainly replaced by hornblende and actinolite, and partially by pyrite, while the plagioclase crystals are strongly altered and replaced by a mixture of blue chlorite and weak, sparse grains of epidote. Ignimbrite samples show a eutaxitic texture with remarkable fiamme and dense welded volcanic glass, along with locally fluidal cryptocrystalline facies, mainly composed of quartz, opaque minerals, sericitized phenocrysts of plagioclase and K-feldspars (Fig. 3i).
- Granodiorite and quartz-diorite samples are grey to light brown, with a moderate pinkish tint related to K-feldspar alteration, and they show a homogenous, coarse-grained texture. Opaque minerals are enclosed in hornblende, biotite and plagioclase. Sericite and clay minerals replace lath-shaped plagioclase phenocrysts and are associated with chlorite and iron oxides (Fig. 3j). Chlorite replaces biotite, which locally substitutes for hornblende crystals. Granite is medium- to locally fine-grained, distinguished from the granodiorite and quartz-diorite by its white to pink color (Fig. 3k).

More details regarding the mineralogical compositions of the studied samples for both Saghro and the Ouarzazate groups are given as Supplementary Table 4.

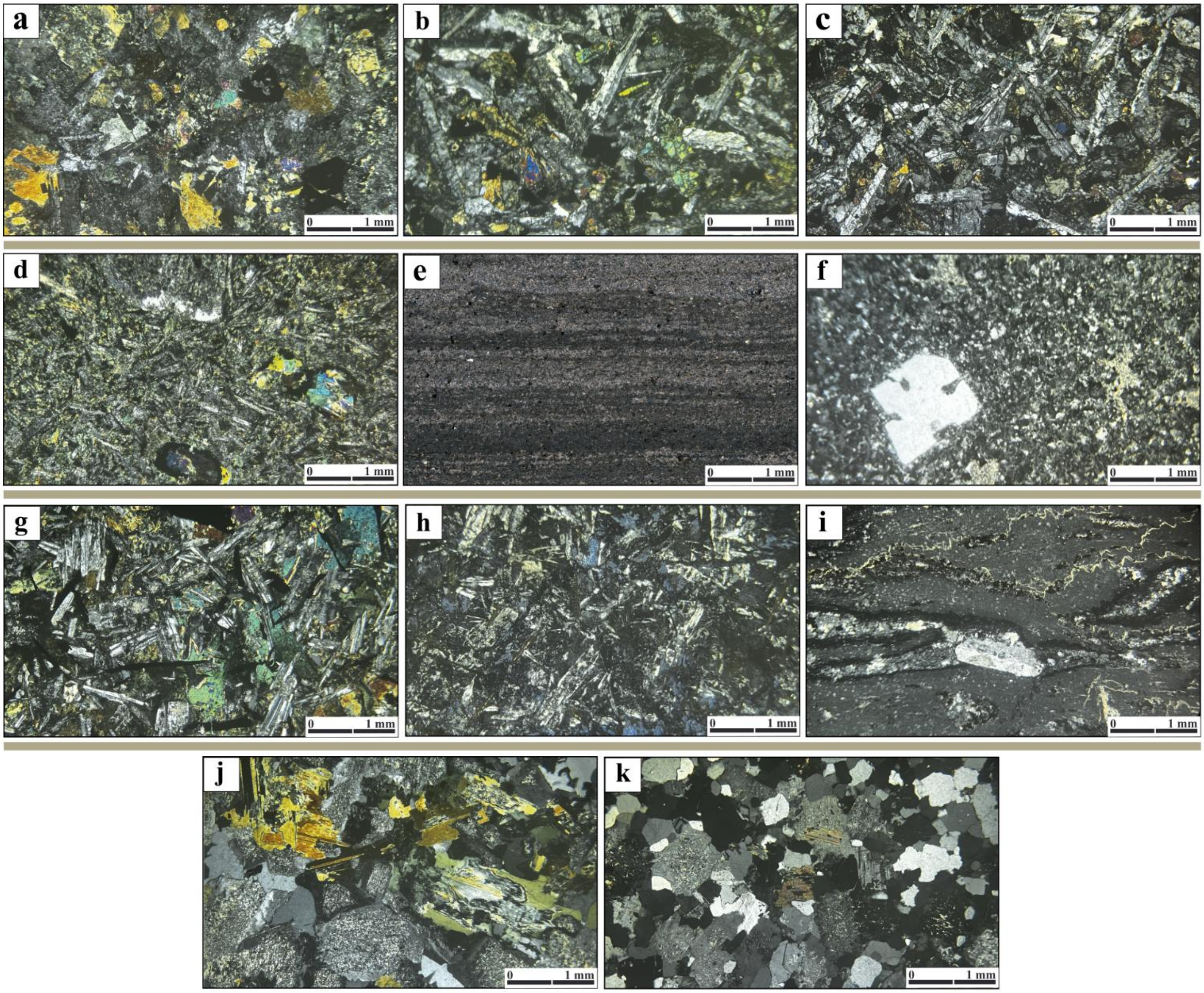

Figure 3. Photomicrographs (all in cross-polarized light) of the studied SG and OG rocks. (a) Gabbro sample showcasing a medium to coarse- grained locally equigranular texture; (b) An intergranular texture for dolerite; (c) Andesite showcasing an ophitic texture; (d) Microlitic-porphyritic texture for basaltic-andesite; (e) Sandstone (Zg-132) exhibiting millimetre-scale laminations showcasing darker bands enriched in chlorite, with quartz-muscovite lighter laminations; (f) Microcrystalline texture for rhyolite with embayed quartz phenocrysts; (g) Dolerite exhibiting an intergranular texture; (h) Diabase characterized by an intergranular texture with patches of blue chlorite; (i) Welded ignimbrite with an eutaxitic texture displaying flow textures with feldspars (sanidine) crystals embedded in a glassy fiamme; (j) Quartz diorite with subhedral to anhedral amphiboles and sericitized plagioclase; (k) Medium to locally fine-grained granite, with an anhedral to subhedral equigranular texture.

4.2 Cathodoluminescence (CL) imaging and LA-ICP-MS U-Pb zircon geochronology

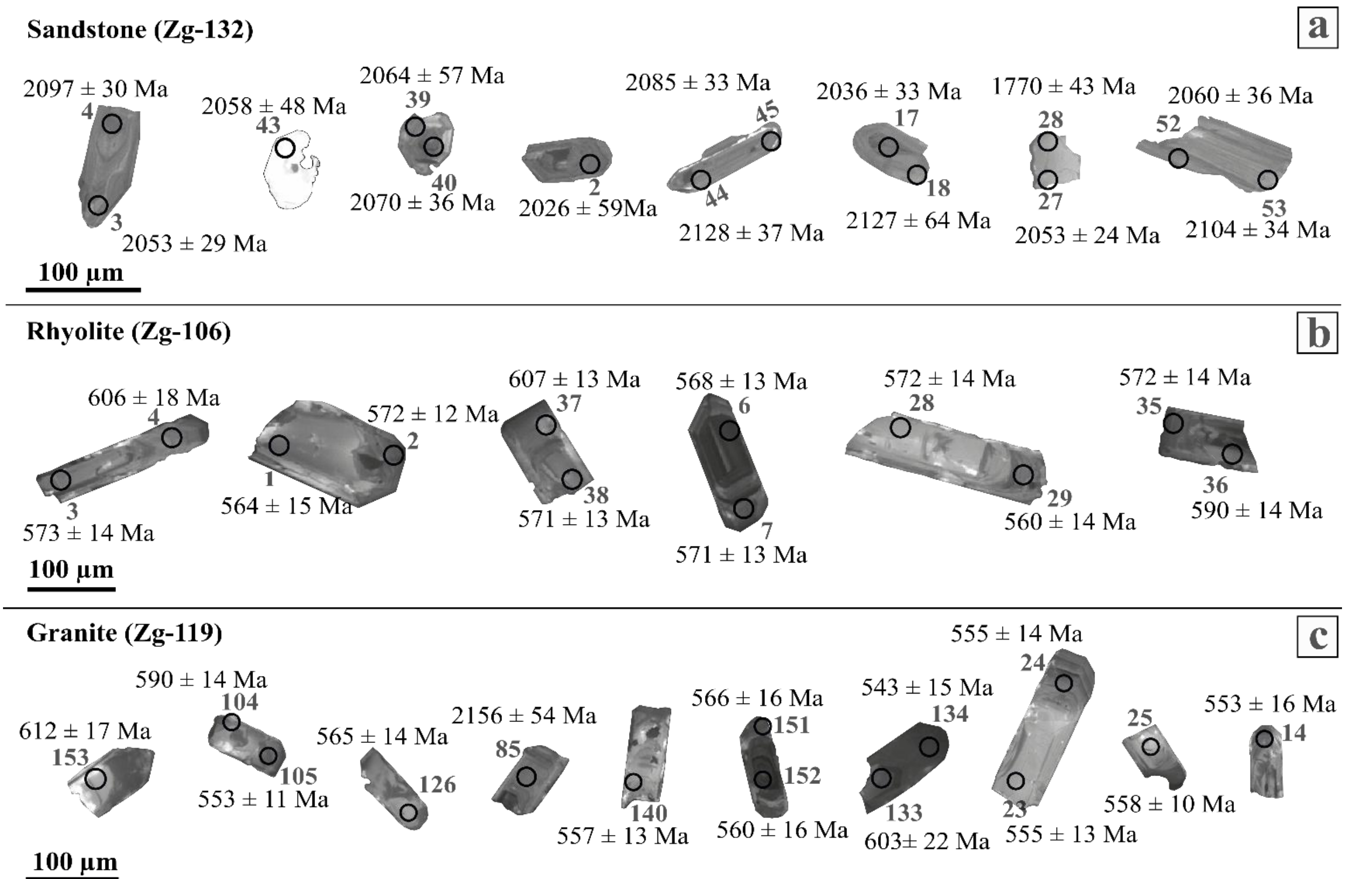

Figure 4. Cathodoluminescence (CL) images of representative zircon grains from the (a): SG sandstone (Zg-132); (b): OG rhyolite (Zg-106); and (c): OG granite (Zg-119). Black circles indicate analytical spots, with corresponding $^{206}Pb/^{238}U$ ages. The reported errors are 2s.

4.2.1 Sandstone (Zg-132)

Most zircons from sample Zg-132 (sandstone) are uniformly rounded and fragmented, with some being subhedral and showing rounded borders. They measure ca. 75–200 µm. They are distinguishable by their low CL signal with some being preferentially zoned (Fig. 4a). A total of hundred and thirty-eight analysis were obtained from ninety-three zircons (rims and cores) from this sample, of which 90 are concordant (Fig. 5A; Supplementary Data 2). The dated zircon grains have Th and U contents of 13–908 ppm and 9–3462 ppm, respectively; Th/U ratios range between 0.03 and 2. For the detrital zircons, we calculated a maximum depositional age (MDA) using the weighted mean of the youngest zircon cluster of three grains with a 98–100% concordance and overlapping in age at 1σ (YC1σ [2+]) (Dickinson and Gehrels, 2009). This yielded a MDA age of 2025 Ma (MSWD = 1.4; n = 3; (Fig. 5A-1)). Moreover, the ages distribution is dominated by one single population, with one uniform peak at 2100 Ma, and one zircon recording an age at 3700 Ma (Fig. 5A-2). The significance of the detrital age will be discussed below (see section 5.4.1).

4.2.2 Rhyolite (Zg-106)

Zircon grains from the Zg-106 (rhyolite) are transparent with subhedral to euhedral habitus. They measure ca. 100–350 µm in length. CL images reveal that zircon grains exhibit typical oscillatory zoning with rare and limited dark rim overgrowths (Fig. 4b). Forty analyses were obtained on twenty-eight zircon grains from this sample (Supplementary data 2). The dated zircon grains have Th and U contents of 20–556 ppm and 40–833 ppm, respectively; Th/U ratios range between 0.3 and 0.7. These data yield a $^{206}Pb/^{238}U$ weighted mean age of 575 ± 3 Ma (MSWD = 1.5; n = 21/40), which is interpreted as the crystallization age of the rhyolite (Fig. 5B).

4.2.3 Granite (Zg-119)

Zircon grains from sample Zg-119 (granite) are mostly euhedral to subhedral with some being rounded. They measure ca. 100–300 µm in length. CL images show visible oscillatory zoning with local moderately fractured zircons showing dark overgrowths (Fig. 4c). A hundred and sixty analyses were obtained on a hundred and twenty-two zircon grains from this sample (Supplementary data 2). The dated zircon grains have Th and U contents of 12–619 ppm and 39–934 ppm, respectively; Th/U ratios range between 0.1 and 1.3, supporting their magmatic origin. Zircon analyses within 95–105% concordance yielded a reliable concordia age of 564 ± 2 Ma (MSWD = 1.6; n = 34/37). One zircon with a $^{206}Pb/^{238}U$ age of 2156 ± 54 Ma (103.5 % concordance) was excluded from the age calculation (Fig. 4c). We also calculated a $^{206}Pb/^{238}U$ weighted mean age using a broader selection of concordant zircons within error, which gave an equivalent age of 564 ± 2 Ma (MSWD = 1.1; n = 76/160) (Fig. 5C). As both ages are statistically identical, we interpret the 564 ± 2 Ma as the crystallization age for the granite.

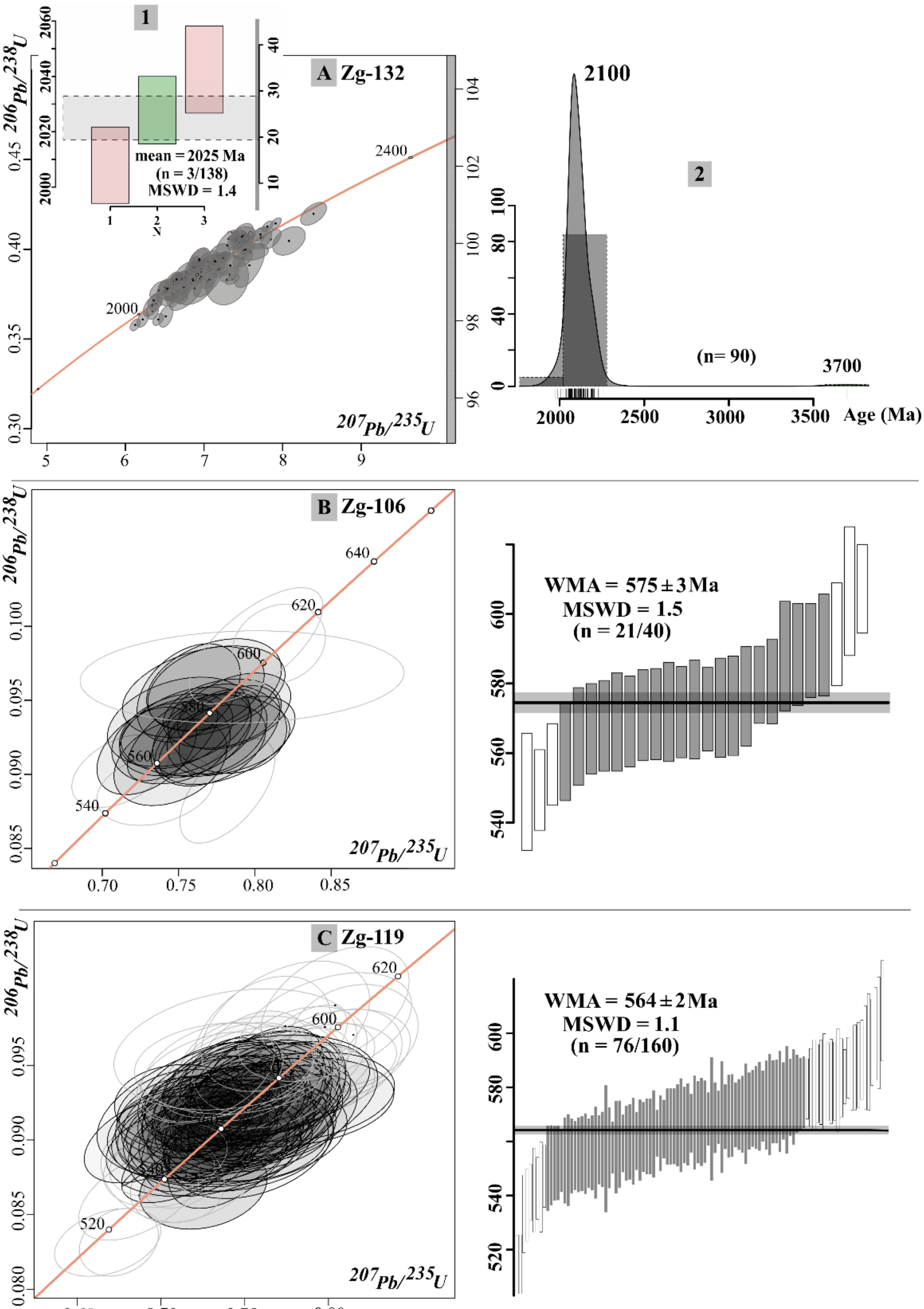

Figure 5. Pb^{206}/U^{238} weighted mean age of three concordant grains, U-Pb concordia, and Kernel Density Estimate (KDE) diagram for (A) Zg-132 (sandstone). Along with U-Pb concordia diagrams, and Pb^{206}/U^{238} weighted mean ages for (B) Zg-106 (rhyolite), and (C) Zg-119 (granite). Ages were calculated using Isoplot R 1.0 (Vermeesch, 2018).

4.3 Whole-rock geochemical compositions

4.3.1 Effects of weathering

Given the samples' distribution and geological diversity, the selected samples are organized according to their lithostratigraphic positions (Supplementary Table 1). Loss on Ignition (LOI) values at 1100 °C are generally low (< 2 wt.%), except for the mafic terms of the SG, which reach approximately 4 wt.% (Supplementary Table 3; n = 32). When plotted on the alteration box plot of Hughes (1972) (Fig. 6a), most samples fall within the igneous spectrum, defining a homogenous hydrothermal trend. However, sample Zg-106 deviates, plotting in the K-altered zone, reflecting localized potassium enrichment. Conversely, two granite samples (Zg-02 and Zg-109) plot in the Na-altered field, suggesting sodium metasomatism.

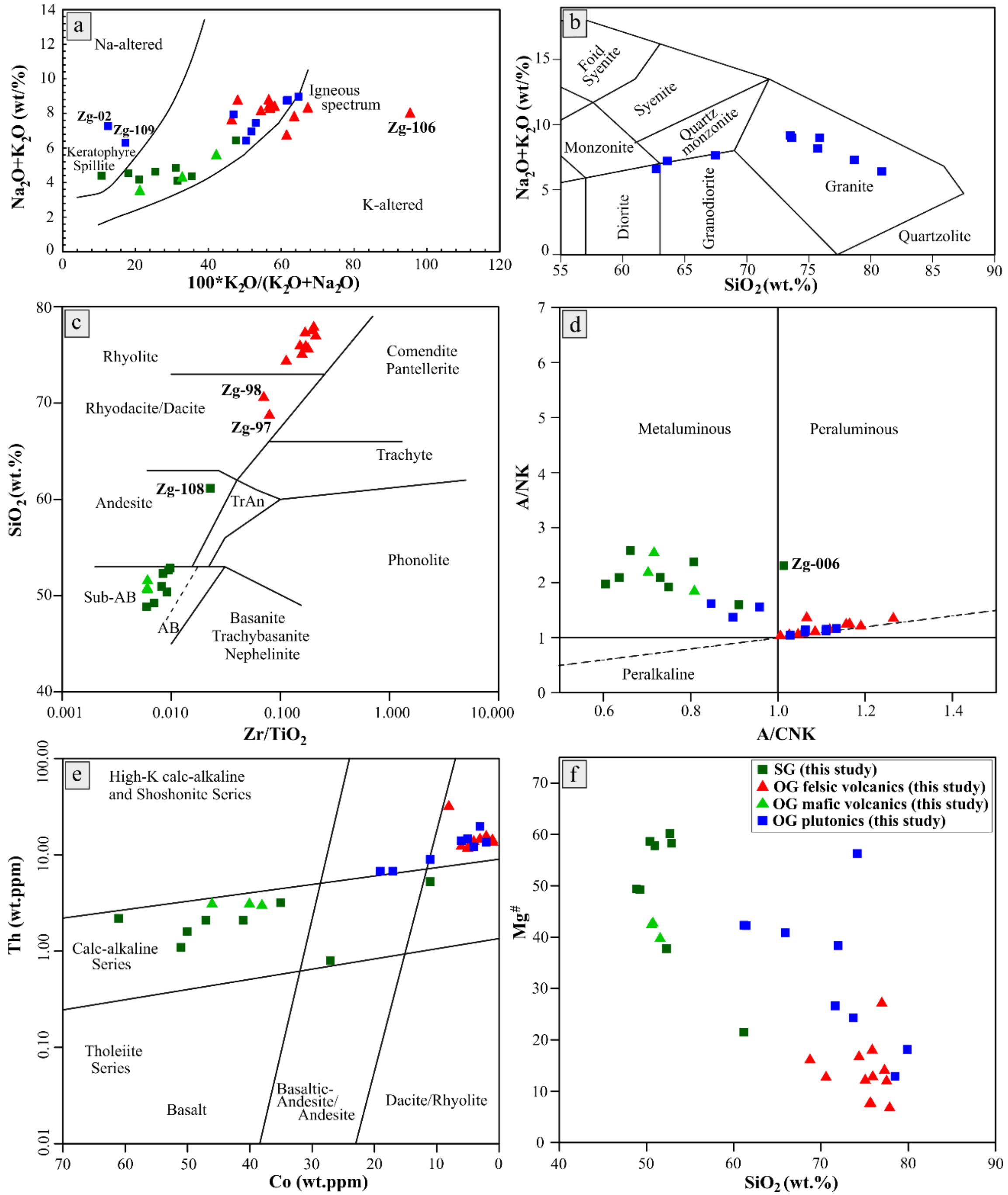

Figure 6. (a) Na_2O+K_2O (wt.%) versus 100*K_2O/(K_2O+Na_2O) plot of Hughes (1972); (b) TAS diagram (after Middlemost, 1994); (c) SiO_2 (wt.%) versus Zr/TiO_2 (Winchester and Floyd, 1977); (d) Plot of A/NK versus A/CNK [A/CNK = molar ratio Al_2O_3 / (CaO + Na_2O + K_2O) and A/NK = molar ratio Al_2O_3 / (Na_2O + K_2O)] (Shand, 1943); (e) Plot of Th (ppm) versus Co (ppm) of Hastie et al. (2007); (f) Mg# value versus SiO_2 contents (wt.%).

4.3.2 The SG magmatic rocks

The analyzed SG rocks belong to the Tittalt Formation in the study area (Fig. 1C; Fig. 2; Thomas et al., 2004, 2002). Geochemically, they define a narrow range of compositions, with SiO_2 contents from 48.85 wt.% to 52.87 wt.%, except for sample Zg-108 with SiO_2 of 61.15 wt.%. They contain 1.08–7.45 wt.% MgO, 13.44–15.65 wt.% Al_2O_3, 2.82–3.95 wt.% Na_2O, and 0.47–3.07 wt.% K_2O. On the SiO_2 (wt.%) vs Zr/TiO_2 diagram, all samples plot within a sub-alkaline basalt field, except sample Zg-108, which has an andesitic composition (Fig. 6c). Most rocks are metaluminous, except sample Zg-006, which is peraluminous (Fig. 6d).The SG rocks also display a calc-alkaline signature (Fig. 6e). Mg# values [Mg# = (MgO+FeO)/MgO×100] range from 21.50 to 60.20 (Fig. 6f).

The SG samples show total rare earth element (∑REE) contents ranging from 60.94 to 231.77 ppm, with coherent patterns characterized by a slight enrichments in light rare earth elements (LREEs) and depletion in heavy rare earth elements (HREEs) (Fig. 7a), with $(La/Yb)_N$ ratios ranging from 1.83 to 6.42 (N denotes normalization to Chondrite). Almost all samples show slight/negligible negative Eu anomalies (Eu/Eu* = 0.89–0.99) to positive one for gabbro Zg-105 (Eu/Eu* = 1.28; Fig. 7a) [Eu/Eu* = 2EuN / (SmN + GdN), where N denotes normalization to chondrite Sm and Gd contents]. On the N-MORB-normalized multi-element diagram (Fig. 7b), the SG rocks show enrichment in large ion lithophile elements (LILEs; e.g., Cs, Rb, Ba, K) relative to high field strength elements (HFSEs), with negative Nb-Ta anomalies and a prominent positive Pb anomaly.

4.3.3 The OG magmatic rocks

The studied samples of the OG are composed of both volcanic and plutonic rocks. The felsic volcanic and plutonic samples have high contents of SiO_2 (61.16–79.89 wt.%), Al_2O_3 (10.83–15.18 wt.%), and CaO (0.1–4.42 wt.%), and low MgO (0.06–2.83 wt.%), Ni (20–60 ppm), and Co (1–19 ppm), except for one granite (Zg-119), which has a relatively high Co content of 109 ppm (Supplementary Table 3). They also have Na_2O+K_2O (wt.%) values of 6.31–8.97, with a K_2O/Na_2O ratio of 0.14–20.75. The plutonic rocks occupy the granite field, with three distinct granodiorite samples (Fig. 6b). Felsic volcanic rocks are as follows: ignimbrites (e.g., Zg-97, Zg-98) classify as rhyodacite and dacite, while rhyolites and rhyolitic-ignimbrites plot within the rhyolite field (Fig. 6c). The whole set consists of peraluminous rocks, except for the granodiorite samples (Zg-07, Zg-08, and Zg-09), which exhibit a metaluminous character (Fig. 6d). They display a high-K calc-alkaline to shoshonitic signature (Fig. 6e).

Mafic volcanics (dolerite) have moderate SiO_2 (50.58–51.56 wt.%), Al_2O_3 (13.9–14.69 wt.%), CaO (5.61–7.67 wt.%), and MgO (4.56–5.3 wt.%) contents. K_2O/Na_2O ratios range from 0.26 to 0.73, with Na_2O+K_2O sums of 3.58–5.64 (Supplementary Table 3). They are sub-alkaline basalts (Fig. 6c), with a metaluminous character (Fig. 6d) and a calc-alkaline signature (Fig. 6e). Mg# values range from 37.19 to 40.16 (Fig. 6f).

The OG samples show total rare earth element (∑REE) contents ranging from 93.52 to 646.17 ppm. In the REE diagram (Fig. 7c), all felsic volcanic and plutonic samples show homogeneous patterns, with LREEs enrichment relative to HREEs. $(La/Yb)_N$

ratios vary between 2.91 and 17.93, except for one rhyolitic sample Zg-106, with a $(La/Yb)_N$ of 0.89. All samples show pronounced negative Eu anomaly (Eu/Eu* = 0.34–0.61), except for sample Zg-106, which exhibits a prominent Eu anomaly (Eu/Eu* = 0.04). In the multi-element spider diagram, all samples display enrichment in LILEs (Cs, Rb, Ba, Th, and U) and depletion in HFSEs (Zr, Nb, Hf and Ta), relative to Primitive Mantle (Fig. 7d). Samples also show prominent negative anomalies in Nb, Ta, P and Ti, along with positive anomalies in Pb, Ba and Th, except for sample Zg-106, which lacks a negative Nb anomaly (Fig. 7d). For the OG dolerites, chondrite normalized REE patterns (Fig. 7c) show moderate LREE enrichment over HREEs, with less fractionated patterns ($(La/Yb)_N$ = 5.94–6.22) and a very low/absent Eu anomaly (Eu/Eu* = 0.88–0.98). However, they are distinguished by a homogenous pattern with prominent Pb enrichment and a less significant Sr anomaly (Fig. 7d).

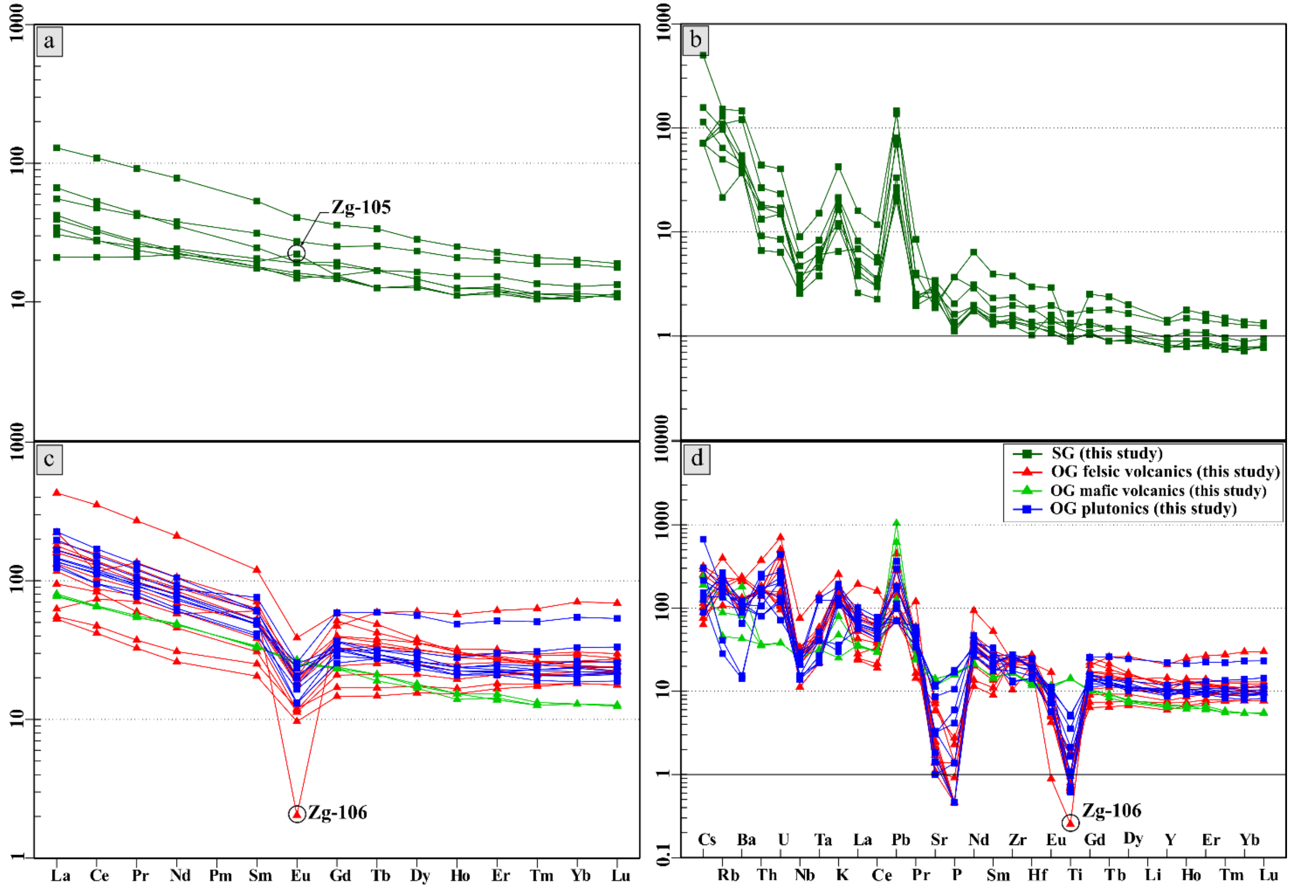

Figure 7. (a) Chondrite-normalized REE diagram of Boynton, (1984) for SG; (b) NMORB normalized diagram of Sun and McDonough (1989) for SG; (c) Chondrite-normalized REE diagram of Boynton, (1984) for OG; (d) Primitive-mantle normalized diagram of Sun and McDonough (1989) for OG.

4.4 Whole-rock Sm-Nd isotope compositions

Sm-Nd isotopic data from seven samples spanning the Ediacaran record of the Sirwa massif reveal petrogenetic processes and orogenic evolution of the Anti-Atlas belt -630–539 Ma) following Bou Azzer-Sirwa ophiolite accretion. Results are listed in Table 1.

Table 1: Whole rock Nd isotopic compositions for the analyzed SG and OG rocks. TDM Goldstein is the Depleted Mantle Age in Ga calculated using the linear model of Goldstein et al. (1984); and is not calculated for samples with $^{147}Sm/^{144}Nd$ ratios greater than 0.145 (Zg-106). Abbreviations: ± 2 SE: Standard Errors (Uncertainty in Nd isotopic composition); N/A : Not Available.

Sample	Lithology	Age (Ma)	Sm (ppm)	Nd (ppm)	$^{147}Sm/^{144}Nd$	$^{143}Nd/^{144}Nd$ measured	± 2SE	$^{143}Nd/^{144}Nd_{(t)}$	$\varepsilon Nd^{(t)}$	TDM (Goldstein) Ga	TDM (2stage) Ga
SG rocks											
Zg-105	Gabbro	620	3.73	13.27	0.1704	0.512762	0.000011	0.512071	+4.6	1.36	0.91
Zg-108	Andesite	620	9.94	40.03	0.1351	0.512550	0.000007	0.512002	+3.2	1.16	1.02
OG rocks											
Zg-09	Granodiorite	570	10.23	50.70	0.1220	0.512414	0.000005	0.511959	+1.1	1.22	1.15
Zg-119	Granite	570	9.10	42.92	0.1283	0.512381	0.000009	0.511903	+0.0	1.37	1.24
Zg-14	Dolerite	570	6.51	28.99	0.1359	0.512390	0.000010	0.511884	-0.3	1.50	1.26
Zg-106	Rhyolite	570	11.50	32.75	0.2124	0.512693	0.000007	0.511902	+0.0	N/A	1.25
Zg-117	Rhyolite	570	10.69	50.59	0.1278	0.512332	0.000011	0.511856	-0.8	1.45	1.30

$$(^{143}Nd/^{144}Nd)_t = (^{143}Nd / ^{144}Nd)_0 + (^{147}Sm / ^{144}Nd)_t \times (e^{\lambda t} - 1)$$

$$\varepsilon Nd^{(t)} = [(^{143}Nd/^{144}Nd_{sample}{}^{t} / ^{143}Nd/^{144}Nd_{CHUR}{}^{t}) - 1] \times 10000$$

$$T_{DM2} = 1/\lambda \times Ln\ \{1 + [(^{143}Nd/^{144}Nd)_{DM} - (^{143}Nd / ^{144}Nd)_{sample} + ((^{147}Sm / ^{144}Nd)_{sample} - (^{147}Sm / ^{144}Nd)_{CC)} \times (e^{\lambda t} - 1)] / ((^{147}Sm / ^{144}Nd)_{DM} - (^{147}Sm / ^{144}Nd)_{CC)}\}$$

$\lambda\ ^{147}Sm = 0.654 \times 10^{-11}\ a^{-1}$: the decay constant of ^{147}Sm.

$(^{143}Nd/^{144}Nd)_{DM} = 0.51315$: present-day ratio of the Depleted Mantle (DM).

$(^{147}Sm / ^{144}Nd)_{DM} = 0.2137$: present-day parent/daughter ratio of the DM.

$(^{147}Sm / ^{144}Nd)_{CC)} = 0.12$: average parent/daughter ratio assigned to the Continental Crust (CC).

Error of initial ratio is calculated from the measurement of error of the isotope ratio, the estimated concentration error and the age error. The decay constant is considered to be a fixed value.

$$\sigma_{Nd(t)} = \sqrt{\sigma_{Nd}^2 + \sigma_{Sm}^2\ (e^{\lambda t} - 1)^2\ + \sigma_t^2\ \left(\lambda e^{\lambda t}\left(\frac{^{147}Sm}{^{144}Nd}\right)\right)^2}$$

$\sigma_{Nd(t)}$ is mean-square deviation of $(^{143}Nd/^{144}Nd)_t$

σ_{Sm} is mean-square deviation of $(^{143}Sm/^{144}Nd)_{sample}$

σ_t is mean-square deviation of age

Based on field relationships, an angular unconformity (Errami et al., 2009; Thomas et al., 2002) marks a significant sedimentary/magmatic gap between the 630–600 Ma SG and the overlaying 570–539 Ma OG (Errami et al., 2021a). We used 620 Ma as a reference age for εNd analyses of SG samples (Zg-105, and Zg-108). They show narrow $(^{143}Nd / ^{144}Nd)$ 620 Ma ratios (~0.512) and positive εNd_{620} values of +3.2 and +4.6. Additionally, the TDM model ages (Fig. 8a) of 1.02 and 0.91 Ga exceed the individual maximum depositional ages of 630–600 Ma, and the crystallization ages of older to contemporaneous igneous intrusions found elsewhere in the Anti-Atlas belt, which fall within 640–580 Ma, (Errami et al., 2021a; O'Connor et al., 2010; Liégeois et al., 2006; Gasquet et al., 2005; Mrini, 1993).

The OG rocks, calculated at 570 Ma, exhibit a mostly uniform distribution, with $(^{143}Nd/^{144}Nd)$ values from 0.5118 to 0.5119. These ratios are close to, or slightly lower than, the Chondritic Uniform Reservoir (CHUR) values. (εNd_{570} = -0.8 to +1.1).

Volcanic rocks show negative to near-zero εNd_{570} values: -0.8 (Tadmant rhyolite), +0.0 (OG rhyolite), and -0.3 (dolerite). Granitoids have εNd_{570} values of +0.0 and +1.1 for Zg-119 and Zg-09, respectively. TDM model ages for all samples range from 1.30 to 1.15 Ga (Fig. 8a). Overall, the distinct $\varepsilon Nd_{(t)}$ isotopic signatures for both groups are further supported by the negative correlation between $\varepsilon Nd_{(t)}$ values and SiO_2 (Fig. 8b).

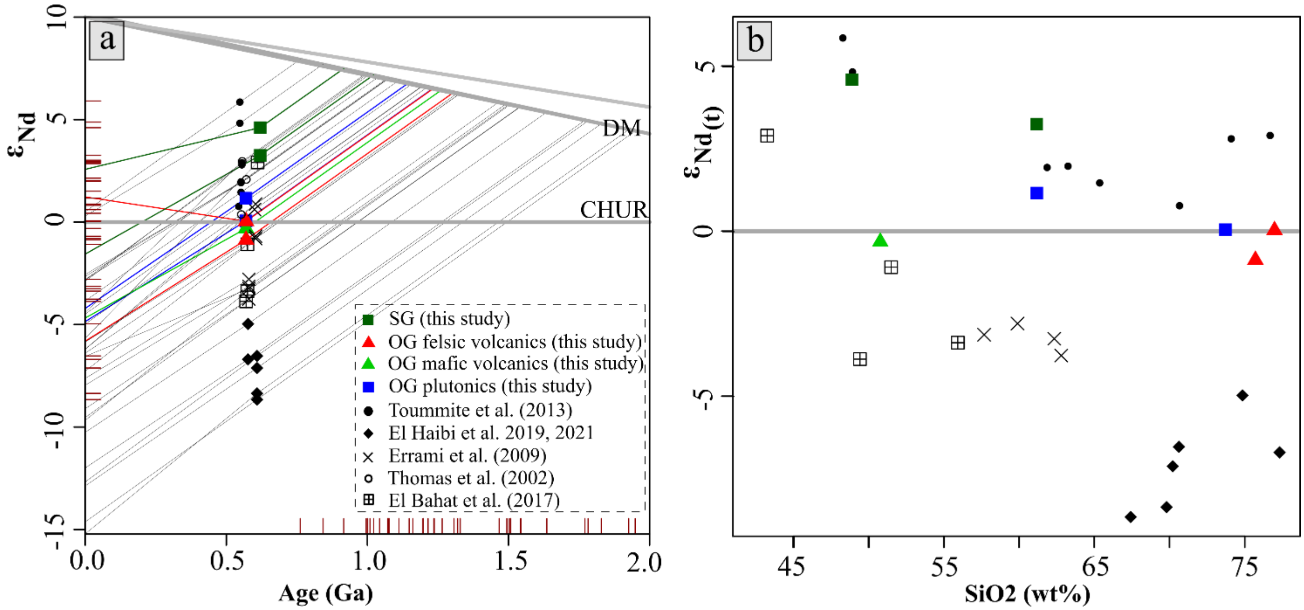

Figure 8. (a) two-stage εNd isotope growth diagram for SG and OG rocks versus Age (Ga). DM, Depleted Mantle evolution lines after Goldstein et al. (1984) and Liew and Hofmann (1988); CHUR, Chondritic Uniform Reservoir. The tick marks on the axes denote two-stage Nd model ages along the x-axis and initial εNd values along the y-axis; (b) Initial εNd versus SiO2 (wt.%) for SG and OG rocks. All samples are compared with selected and available reference rocks from the literature. Calculations and diagrams are produced using GCDkit (Janoušek et al., 2006).

Further, to quantify the mixing proportions for the Saghro and Ouarzazate groups, this study employs a binary mixing model based on the equations of Faure (1986), following the computational approach detailed by Janoušek et al. (2016). In this model, the isotopic ratio of a mixture (I_M) is defined as the mean of the isotopic ratios of two end-members (I_1 and I_2), weighted by their respective mass fractions and elemental concentrations. f_1 represents the mass fraction of end-member 1 (where $f_1 + f_2 = 1$), while C_1, C_2, and C_M represent the elemental concentrations of the end-members and the resulting mixture, respectively. Mantle end-member 1 is defined by a metasomatized lithospheric source, with values of $I_1 = 0.512265$, $C_1 = 13.27$ ppm, and $\varepsilon Nd_{620} = +8$ from Errami et al. (2009), reflecting mantle enrichment by prior subduction processes. For crustal end-member 2, we used parameters from Ennih and Liégeois (2008) ($I_2 = 0.511472$; $C_2 = 47$ ppm; $\varepsilon Nd_{620} = -16$), representing the Paleoproterozoic basement of the WAC.

The mixing equations are defined as:

$$I_M = I_1 \left(\frac{C_1}{C_M}\right) f_1 + I_2 \left(\frac{C_2}{C_M}\right) (1 - f_1)$$

Where:

(1)

$$C_{\mathrm{M}} = f_1 C_1 + (1 - f_1) C_2$$

(2)

$$f_1 = \frac{C_2(\mathrm{I_M} - \mathrm{I_2})}{C_1(\mathrm{I_1} - \mathrm{I_M}) + C_2(\mathrm{I_M} - \mathrm{I_2})})$$

Applying this mixing model reveals that SG rocks are characterized by a dominantly mantle origin: the andesite (Zg-108) and gabbro (Zg-105) yield high mantle-derived mass fractions (f_1) of 88 % and 92 %, respectively, with minor crustal inputs ($f_2 \approx$ 8 % –12 %). Conversely, the OG magmas have mantle mass fractions (f_1) ranging from 75 % to 85 %. Moreover, the calculated crustal contribution (f_2) increases from 15 % in granodiorite (Zg-09) to 25 % in rhyolite (Zg-117).

5 Discussion

5.1 Petrogenesis

The SG and OG rocks exhibit chemical evolution consistent with fractional crystallization. General trends for major elements (e.g., Al_2O_3, CaO, and TiO_2) show positive correlations with Mg# (Fig. 9a,b, and c). Al_2O_3 contents decrease with decreasing Mg# suggesting plagioclase crystallization (Fig. 9a). CaO contents drop sharply as Mg# decreases below ~40, indicating clinopyroxene or calcic plagioclase fractionation (Fig. 9b). TiO_2 also decreases with decreasing Mg#, pointing to early crystallization of Fe-Ti oxides (e.g., ilmenite or titanomagnetite) (Fig. 9c).

On the A/CNK versus Mg# plot (Fig. 9d), the SG rocks are metaluminous (A/CNK < 1.0), while the OG felsic and plutonic rocks are peraluminous (A/CNK > 1.0). This shift to peraluminous compositions suggests melting of aluminum-rich material or fractionation of aluminum-poor minerals (e.g., hornblende, pyroxene) in the felsic rocks. In Figure. 9e, the SG rocks retain the highest Sr concentrations (~200–350 ppm), indicating a more aluminum-enriched source or less plagioclase removal. This is supported by the absence of a negative Eu anomaly (Eu/Eu* = 0.89–1.28), reaching a positive value for gabbro Zg-105 (Eu/Eu* = 1.28), indicating limited plagioclase fractionation (Fig. 7a). In contrast, the OG rocks show a marked Sr decline from mafic volcanics through plutonics to felsic volcanics, indicating that plagioclase crystallization was the dominant driver of OG differentiation (Fig. 9e). This is corroborated by the prominent negative Eu anomaly in rhyolite Zg-106, while the absence of an Eu anomaly in dolerites suggests limited plagioclase involvement (Fig. 7c).

On the Th (ppm) versus Mg# plot (Fig. 9f), both the SG rocks and OG mafic volcanics show low Th concentrations (<5 ppm), typical of mantle-derived melts. For the SG, however, Mg# values of 21.50 to 60.20 reflect early fractionation of ferromagnesian minerals, indicating the rocks are not derived from a primitive melt. For the OG, Th levels reach up to 32 ppm in felsic volcanics and plutonics, suggesting crustal melting or assimilation during magma ascent (Fig. 9f). The absence of a negative Eu anomaly in the SG rocks (Fig. 7a), despite the evolved nature of the magmas, likely reflects mixing between evolved basaltic magmas and more primitive magmas that lacked plagioclase fractionation. The OG felsic volcanics and plutonics show Sr and P depletion, consistent with plagioclase and apatite fractionation (Fig. 7d).

Eu/Eu* values versus Sr contents (ppm) show a clear positive correlation (Fig. 9g). Mafic rocks of the Saghro and the Ouarzazate groups have high Sr and Eu/Eu* values near 1.0, suggesting plagioclase accumulation consistent with their more primitive nature. In contrast, the OG felsic volcanics and plutonics show significantly lower Sr and Eu/Eu* values, indicating substantial plagioclase fractionation from the melt (Fig. 9g). Whole rock Zr/Sm versus Zr and Rb/Nb versus Rb correlations are as expected for a fractional crystallization process (Fig. 9h-i). A localized spike in Zr/Sm at high Zr contents (~350 ppm) indicates late-stage mineralogical control, involving zircon or amphibole fractionation in the more evolved OG, distinct from the relatively stable ratios of most samples (Fig. 9h). This implies that the magmatic evolution of the SG and the OG rocks involved both fractional crystallization and progressive crustal contamination or a subduction-modified source (Fig. 9i).

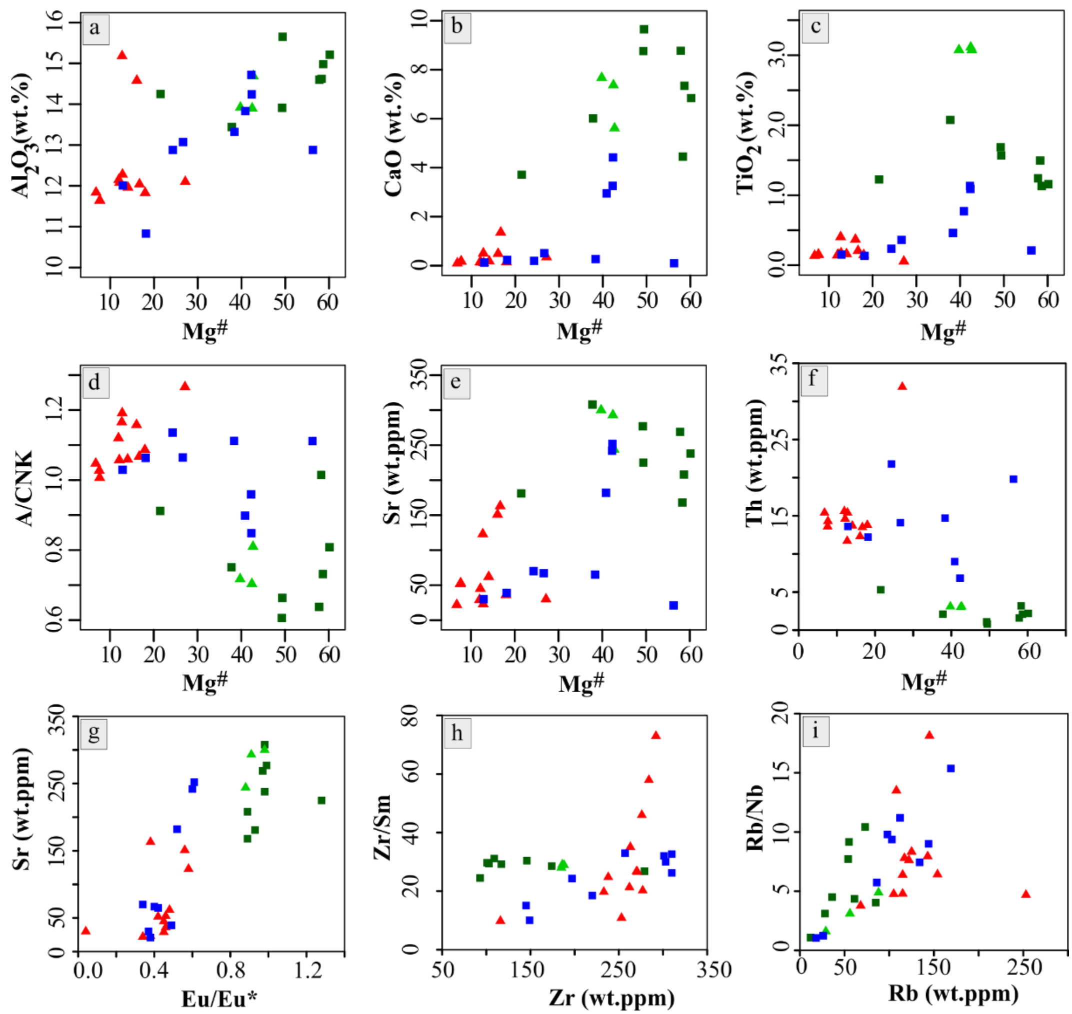

Figure 9. (a) Al_2O_3 (wt.%) versus Mg#; (b) CaO (wt.%) versus Mg#; (c) TiO_2 (wt.%) versus Mg#; (d) A/CNK (A/CNK = molar ratio Al_2O_3 / (CaO + Na_2O + K_2O)) versus Mg#; (e) Sr (ppm) versus Mg#; (f) Th (ppm) versus Mg#; (g) Zr / Sm value versus Zr content (ppm); (h) Rb / Nb value versus Rb content (ppm); (i) Eu / Eu* value versus Sr (ppm). Symbols as those in Figure 6.

The εNd_i versus $^{147}Sm/^{144}Nd$ plot clearly distinguishes the SG from the OG rocks (Fig. 10a). The SG rocks show strongly positive εNd_i values (+3.2 and +4.6), indicating a juvenile, depleted mantle origin with minimal crustal interaction. In contrast, the OG rocks, by contrast, cluster near or below the CHUR line (εNd_i = -0.8 to +1.1), reflecting a hybrid source with significant reworking of older continental crust. Sample Zg-106 shares this near-zero isotopic signature, but its unusually high $^{147}Sm/^{144}Nd$ ratio (~0.21) points to a distinct petrogenetic process, likely low degree of partial melting that fractionated REE without significantly altering the initial Nd isotopic composition of its source (Fig. 10a).

The SG and OG also show are distinct geochemical fingerprints. For samples with Nb < 25 ppm (Fig. 10b), Nb/Ta ratios show a wide spread (~3–15): OG plutonics decline sharply (~3), indicating advanced fractional crystallization of ferromagnesian and accessory minerals, while SG mafic rocks maintain higher, stable ratios (~10–15), consistent with more primitive melts. Although Nb and Ta typically behave as geochemical twins, they can fractionate during subduction (Hofmann et al., 1986). The OG rocks cluster below a Nb/Ta ratio of 14, well below the mantle value of 17.5 (Sun and McDonough, 1989) and close to the bulk continental crust value of ~11 (Green, 1995), confirming a dominant crustal signature. This is further corroborated by an enrichment in LILEs), coupled with prominent negative Nb-Ta and Ti anomalies (Fig. 7d), consistent with subduction-related magmatism or recycling of metasomatized lithosphere (Ikenne et al., 2007). Finally, the OG rhyolite (Zg-106) displays a horizontal shift toward higher Nb at a fixed Nb/Ta ratio (~9) (Fig. 10b), suggesting magma enrichment via a low degree partial melting from a source already characterized by a low Nb/Ta ratio and a pre-existing subduction-modified signature.

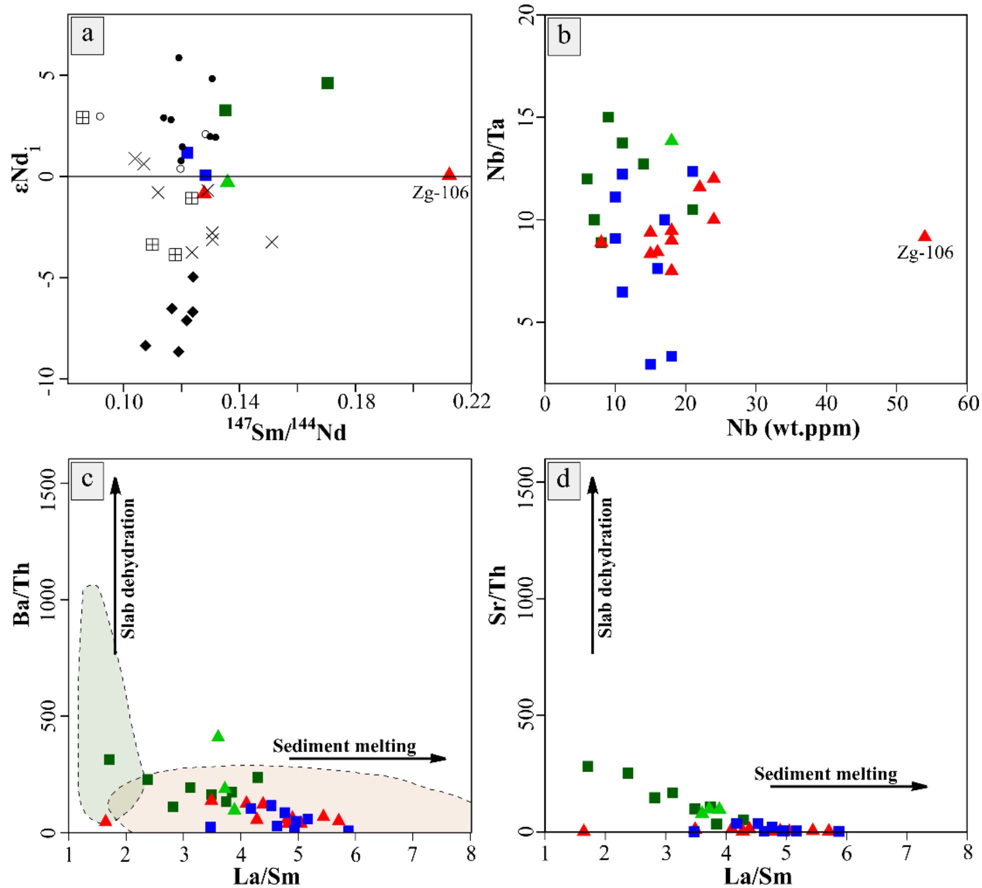

Figure 10. Plots (a) Initial εNd versus ^{147}Sm/^{144}Nd; (b) Nb/Ta versus Nb contents (ppm); (c) Ba/Th versus La/Sm and (d) Sr/Th versus La/Sm (domains are modified from Labanieh et al. (2012). Legend is the same as in Figure 8.

The SG and OG rocks show enrichment in LILEs and LREEs relative to HFSEs and HREEs. They also exhibit pronounced negative anomalies in Nb, Ta, and Ti (Fig. 7), suggesting subduction zone fluids influence (Wilson, 1989). For the OG rocks, this inherited geochemical signature is attributed to oceanic arc rocks previously subducted into the mantle (Toummite et al., 2013; Gasquet et al., 2008; Ikenne et al., 2007; Thomas et al., 2002).

Trace elements can clarify subduction input versus crustal contamination. In the Ba/Th versus La/Sm diagram (Fig. 10c), most samples display low Ba/Th and high, variable La/Sm ratios, favoring a dominant role for sediment melting process. A similar sediment melt signature is also observed for all samples in the Sr/Th versus La/Sm diagram (Fig. 10d). For the SG rocks, relatively high Sr/Th ratios are attributed to plagioclase accumulation. High La/Sm ratios further indicate a sediment-dominated influence, suggesting that slab pressure-temperature conditions were sufficient to trigger sediment melting (Labanieh et al., 2012). This melting process acted as the primary mechanism transferring the slab signature into the analyzed samples.

5.2 Initial Sm-Nd isotopes composition and magma source characteristics

The whole-rock Sm-Nd isotope compositions of the Saghro and Ouarzazate groups suggest a heterogeneous magma source, reflected in the negative correlation between $\varepsilon Nd_{(t)}$ values and SiO2 (Fig. 8b). The SG maintains high $\varepsilon Nd_{(620)}$ values (+3.2 and +4.6) even as silica increase, reinforcing a juvenile mantle source with minimal crustal input,. The corresponding TDM model ages of 1.02 and 0.91 Ga further support a depleted mantle source. Within the OG, the decreasing trend in εNd_{570} = +1.1 to -0.8 with increasing SiO_2 is a classic signature of Assimilation-Fractional Crystallization (AFC), whereby the cooling magma evolves toward a felsic composition while incorporating more evolved, negative εNd continental crust. Notably, TDM model ages clustering around 1.30 to 1.15 Ga indicate that the OG magmas were not purely mantle-derived, but involved significant recycling of much older basement (Mesoproterozoic and/or Paleoproterozoic).

The binary mixing model validates these isotopic trends. The SG rocks show a near-pristine mantle signature (f_1 = 88–92 %). However, the increasing crustal contribution (f_2) of the OG rocks, from 15 % in granodiorite (Zg-09) to 25 % in rhyolite (Zg-117), confirms a coupling between increasingly felsic compositions and higher crustal input. This 25 % contribution from an ancient Paleoproterozoic source (εNd_{620} = -16) represents a major contamination event, exerting a significant isotopic pull by shifting the εNd values of the samples to near zero. Normally, without recycling of this ancient basement, a purely mantle-derived magma at 570 Ma would be expected to show strongly positive values of +7 to +8. This hybridization is further supported by the TDM model ages of 1.30 to 1.15 Ga, proving the significant involvement of the underlying Eburnean WAC basement.

5.3 Tectonic implications

Previously, the SG basin was interpreted as consisting of distal, deep marine sediments equivalent to the platform series of the Tachdamt Group, formed during initial rifting associated with the Rodinia breakup (Thomas et al., 2002). However, recent zircon data from SG sediments in the Sirwa and Saghro inliers suggest deposition occurred following Bou Azzer–Sirwa ophiolite accretion, during the main Pan-African Orogeny (Abati et al., 2010; Errami et al., 2009; Liégeois et al., 2006). Furthermore, the tectonic setting of Ediacaran OG magmatism also remains debated, having been interpreted as: (i) post-collisional, linked to asthenospheric upwelling beneath the WAC during its metacratonic evolution (Gasquet et al., 2008, 2005; Liégeois et al., 2006; Thomas et al., 2002); (ii) subduction related (Walsh et al., 2012; Benziane, 2007; El Baghdadi et al., 2003); or (iii) linked to Iapetus Ocean opening, tied to the Ediacaran Central Iapetus Magmatic Province (CIMP; Youbi et al., 2020). Based on age and chemical similarities, this magmatism is also associated with the Avalonian-Cadomian marginal belt along the northwestern edge of Gondwana, constituting a major magmatic flare-up spanning roughly 590–540 Ma (Letsch et al., 2018; Tahiri et al., 2010; Linnemann et al., 2008).

For our samples, multi-elemental discrimination plots (Fig. 11a–f) provide a framework for deciphering the petrogenesis and tectonic transition of Ediacaran magmatic sequences in the Anti-Atlas. First, the SG basalts feature high Zr and relatively low Y concentrations, classifying them as within-plate basalts (WPB) (Fig. 11a) and indicating an extensional to transtensional setting. On the Th/Nb versus Ti/V diagram of Shervais (2022), these samples plot within the Continental Flood Basalts (CFB) field (Fig. 11b). Placed in the regional context of the Anti-Atlas, the geodynamic setting of the SG has been interpreted as an intracontinental rift evolving into either a mature back-arc basin (Errami et al., 2009; Fekkak et al., 2001) or a continental passive margin (Fekkak et al., 2002). This evolution is characterized by a transition from early, sediment-influenced tholeiites to more evolved magmatic suites, rather than a massive subaerial flood province. The calc-alkaline character for the SG mafic rocks (Fig. 6e) reflects Th enrichmentt, typical of subduction-influenced or crustally contaminated suites. This transitional character, exhibiting calc-alkaline affinity (Fig. 6e), yet within-plate (Fig. 11a) and continental tholeiites (Fig. 11e) character is interpreted as an early Ediacaran extensional phase, where advanced lithospheric thinning allowed asthenospheric decompression, triggering large-scale melting of the Sub-Continental Lithospheric Mantle (SCLM). In contrast, the younger OG volcanic and plutonic rocks plot at higher Th/Nb ratios (>0.5),within the Upper Continental Crust (UCC) and Andean Arc fields, with extreme Th enrichment pointing to a regional thermal regime shift (Fig. 11b). This OG magmatism marks a massive crustal melting event, interpreted as a response to post-collisional lithospheric delamination and possible slab break-off. This process generated highly differentiated magmatic suites with wide variations in Ti/V ratios (Fig. 11b).

Furthermore, there is a clear lithospheric distinction between the SG and the OG rocks based on trace element enrichments. The SG mafic rocks follow the MORB-OIB array (Fig. 11c), indicating a magma source akin to enriched mid-ocean ridge basalt (E-MORB). This implies that primary magmas were derived via partial melting of an enriched lithospheric mantle carrying a fossil subduction signature from earlier Cryogenian cycles. Conversely, the younger OG volcanic and plutonic rocks show considerable crustal contamination. Their shift toward higher Th/Yb ratios reflects input of continental crust, or widespread tapping of a SCLM domain deeply metasomatized by subduction-related sediments (Fig. 11c). The SG rocks' lower Th/Nb ratios further suggest a more primitive, mantle-dominated source modified by an ancient subduction-preconditioned lithospheric root rather than an active deep-mantle plume head, clustering within the vertical Subduction Zone-Modified Lithospheric Mantle (SZLM) array, near the LCC (Lower Continental Crust) (Fig. 11d).

The OG rocks, in contrast, plot within the upper limits of the SZLM array, clustering within the IAB and CAB fields. This geochemical footprint may signify slab break-off, whereby crustal recycling or melting of the thickened lithospheric root was driven directly by the thermal anomaly of the upwelling asthenospheric mantle (Fig. 11d).

Ultimately, a coherent geodynamic transition emerges between both Saghro and Ouarzazate groups. On Figure. 11e, the SG mafic rocks cluster within the Continental Tholeiites (CT) field, adjacent to the Back-Arc Basin (BAB) domain. This position, combined with their calc-alkaline signature and within-plate character noted above, supports formation in an extensional continental setting. The proximity to the BAB field suggests that, while the crust was thinning, the magmatism retained a slight transitional character typical of a maturing continental rift or back-arc basin, with a distinct geochemical overprint from a pre-modified lithospheric root. The OG felsic and plutonic samples, meanwhile, plot decisively within the A2-type granite field, supporting a post-collisional origin (Fig. 11f). A2-type granites are considered to originate from partial melting of continental or underplated mafic crust, typically in extensional settings (Eby, 1992). In this context, crustal recycling was likely driven by the mechanical and thermal effects of lithospheric delamination and potential slab failure (Blein et al., 2023; Ougadire et al., 2023). This triggered rapid basin development and accumulation of the thick volcano-sedimentary sequences characteristic the OG, across the already rigid, fractured metacratonic margin of the WAC, providing preferential pathways for the rapid upward migration of deep-sourced magmas (Walsh et al., 2012, and references therein; Ennih and Liégeois, 2001, 2008; Gasquet et al., 2008).

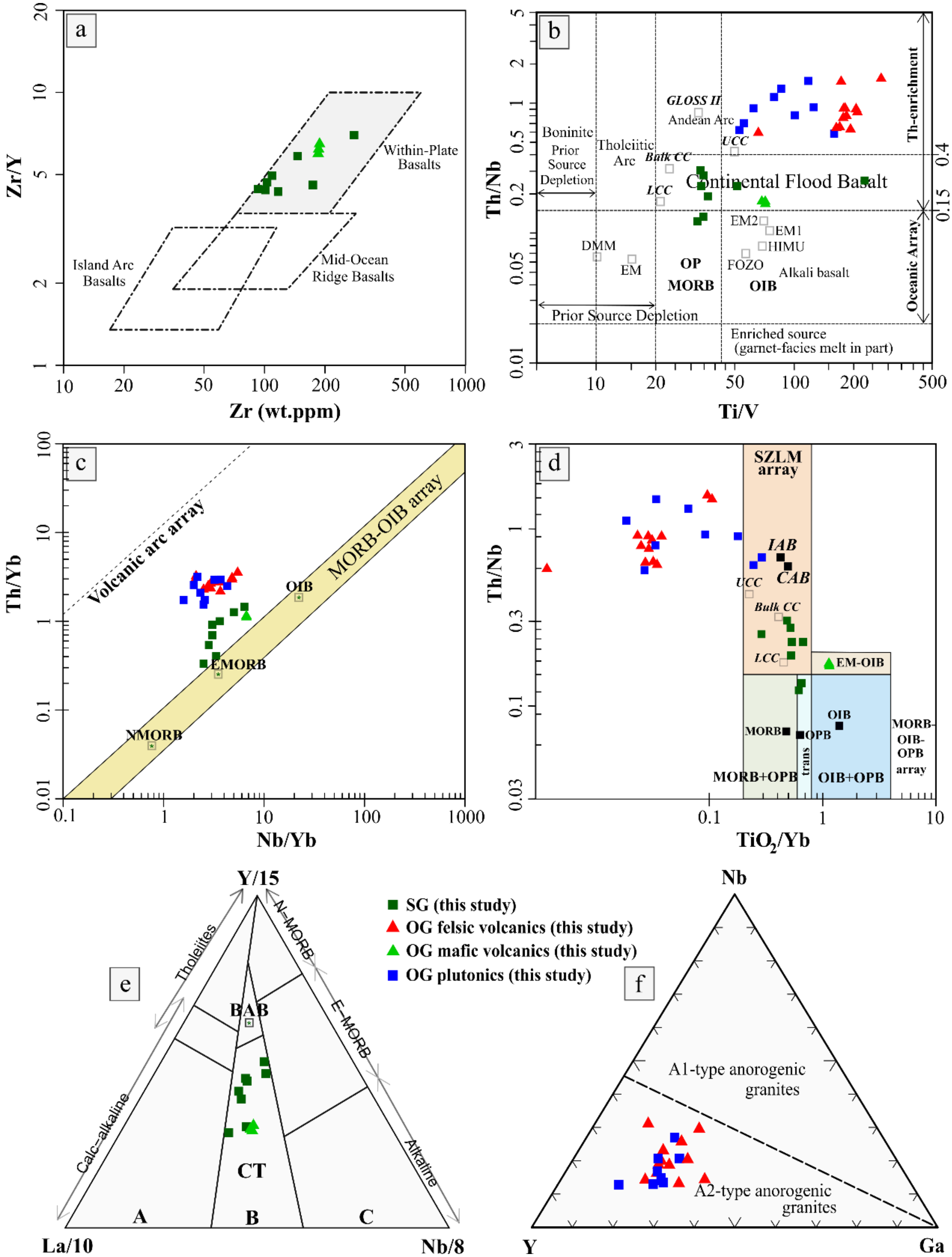

Figure 11. (a) Zr/Y vs Zr (ppm) plot for SG rocks and OG mafic volcanics (Pearce and Norry, 1979); (b) Th/Nb versus Ti/V diagram of Shervais (2022); (c) Th/Yb versus Nb/Yb diagram of Pearce (2008); (d) Th/Nb versus TiO_2/Yb plot of Pearce et al. (2021); (e)

La/10 – Y/15 – Nb/8 ternary diagram for the tectonic discrimination of basaltic rocks (Cabanis and Lecolle, 1989); (f) Nb – Y – Ga ternary diagram for the classification of A1 and A2-type anorogenic granites (Eby, 1992). Abbreviations: Bulk CC: Bulk Continental Crust; GLOSS: Global Subducting Sediment; LCC: Lower Continental Crust; UCC: Upper Continental Crust; EM1 / EM2: Enriched Mantle (Type 1 & 2); DMM: Depleted MORB Mantle; HIMU: High μ (high $^{238}U/^{204}Pb$ ratio) mantle reservoir; OIB: Ocean Island Basalt; SZLM: Subduction Zone-Modified Lithospheric Mantle; CAB: Calc-Alkaline Basalt; IAB: Island Arc Basalt; OPB: Oceanic Plateau Basalt; MORB: Mid-Ocean Ridge Basalt; N-MORB: Normal Mid-Ocean Ridge Basalt; E-MORB: Enriched Mid-Ocean Ridge Basalt; EM: Enriched Mantle; OP MORB: BAB: Back-Arc Basin; CFB: Continental Flood Basalt; CT: Continental Tholeiites; A: Orogenic (compressive) domains (island arc, active margins); B: Late to post-orogenic (compressive to distensive) intra-continent domains; C: Anorogenic (distensive) domains.

5.4 Significance of LA-ICP-MS U-Pb data

5.4.1 The SG detrital age

The existence of Paleoproterozoic basement in the Sirwa massif and the northern margin of the WAC remains debated (Ennih and Liégeois, 2008). While traditionally thought to be confined to the Western Anti-Atlas (Choubert, 1963), recent studies suggest Paleoproterozoic rocks may also be present in the Central and Eastern Anti-Atlas and the Western Meseta (Liégeois et al., 2013; Abati et al., 2010; Gasquet et al., 2008; Pereira et al., 2015, and references therein; Blein et al., 2014). Historically, the WAC's northern boundary was defined by the deformed Tazagzaout migmatites and gneisses in the Bou-Azzer inlier (Leblanc and Lancelot, 1980). However, new U-Pb dating of the Tazagzaout gneisses (752 ± 2 Ma; D'Lemos et al., (2006) and the Oumlil granite (741 ± 9 Ma; El Hadi et al., 2010), coupled with juvenile Nd signatures (D'Lemos et al., 2006), indicates a juvenile, depleted mantle source, not akin to the 2 Ga Eburnean WAC basement.

According to Thomas et al. (2002), the Imghi Formation represents the lower, thick bedded greywacke/turbiditic section of the SG, forming a typical flysch succession interpreted as the primary sedimentary fill of a back-arc basin associated with the Khzama ophiolite Complex. For Zg-132, the alternating patterns (Fig. 3e) suggest fluctuating depositional conditions, specifically changes in hydrodynamic energy and the amount of clay input, consistent with a low-energy, suspension-dominated sedimentation typical of distal turbidites or quiet shallow-marine environment. The calculated MDA of 2025 Ma (n= 3; MSWD = 1.4; Fig. 5A-1) is similar to ages of syn-to-post-tectonic Eburnean granites in the Central and Western Anti-Atlas (Gasquet et al., 2008, 2005; Aït Malek et al., 1998). The detrital zircon age distribution is further characterized by a prominent population peaking at ca. 2100 Ma (Fig. 5A-2), reflecting a dominant provenance from the Eburnean-aged WAC basement (O'Connor et al., 2010; Gasquet et al., 2008, 2005; Thomas et al., 2002). This primary pulse, coupled with a single Paleo-Archean grain at 3700 Ma, indicates recycling of ancient cratonic material (Fig. 5A-2). Interestingly, no ages younger than 1600 Ma were found in our sample; in particular, 883–640 Ma Pan-African zircons, which are common in outcrops of the Sirwa inlier and consistently reported in SG sediments elsewhere (Letsch et al., 2018; Abati et al., 2010), are absent. The narrow gap between the 2100 Ma peak and the 2025 MDA suggests that sedimentation occurred in a basin directly overlaid or adjacent to an uplifted, pristine block of Paleoproterozoic Eburnean basement, which acted as the exclusive sediment source without interaction with Ediacaran sediments.

The returned age may reflect insufficient sampling of detrital zircons; however, the number of analyzed zircons (up to 138; Supplementary Table 2) is considered adequate to address paleogeographic questions and sediment source provenance

(Vermeesch, 2004). Based on these findings, the WAC crust likely extends beneath the Sirwa massif and continues northward well beyond the Anti-Atlas belt. Notably, Paleoproterozoic rhyolites have also been reported in the Meseta Block, north of the Anti-Atlas, with a magmatic age of 2050.6 ± 3 Ma (Pereira et al., 2015). These findings do support the presence of WAC Paleoproterozoic crust northward beyond the AAMF.

5.4.2 Magmatic record on the OG

New U-Pb zircon dating of two magmatic samples (rhyolite Zg-106, and granite Zg-119; Fig. 4), representing the OG in the Sirwa massif, returned ages of 575 ± 3 Ma and 564 ± 2 Ma, respectively. These ages are consistent with a lower OG affinity, representing an expression of the Ediacaran magmatism previously described across numerous inliers of the Anti-Atlas belt (Yajioui et al., 2020; Walsh et al., 2012; Gasquet et al., 2005; Thomas et al., 2002).
In the ZGMR, similar volcanic activity of this type can be bracketed between 620 and 550 Ma (Pelleter et al., 2016; Thomas et al., 2002; this study). Pelleter et al. (2016) reported a mean age of 578 ± 4 Ma for rhyolitic dikes and plugs at the Zgounder Mine, using the ^{207}Pb/^{206}Pb ages. In the Sirwa massif, similar U-Pb ages of 579 ± 7 Ma, 571 ± 8 Ma, 577 ± 6 Ma, 579 ± 7, and 575 ± 8 Ma were obtained for the Tourcht diorite, the Tikhfist rhyolite (Tiouin Subgroup, Fig. 1C), the Aguins member (Tafrant Subgroup), the Tilsakht granite, and the Askaoun granodiorite, respectively (Thomas et al., 2002). Given that our rhyolite's age of 575 ± 3 Ma is identical within error to these ages, a rapid sequence of intrusive events had to occur within a few million years.
For the granite sample (Zg-119), the obtained age of 564 ± 2 Ma is also identical within error to the ages of the neighbouring Imourkhssen granite, dated respectively at 561 ± 3 Ma, 562 ± 5 Ma, and 558 ± 1 Ma by Toummite et al. (2013), Thomas et al. (2002), and Ferraq et al. (2024) (Fig. 1C). The Imourkhssen granite intrudes the lower, older part of the OG in the Sirwa massif (Thomas et al., 2002). Additionally, numerous syn- to late-OG granites in the Sirwa massif have similarly yielded ages of c. 560 Ma, making them the youngest components of the OG (Thomas et al., 2002). According to Thomas et al. (2002), these granites belong to the Achkoukchi Complex (Fig. 1C) and are grouped into the Amassine Suite (e.g., Bou-Tazart, Aït Nabdas, and Tikitar granites, and the Tazoult Quartz-porphyry at 559 ± 6 Ma). The inherited age of 2156 ± 54 Ma in sample Zg-119 indicates a Paleoproterozoic crustal component, supporting reworking of ancient Eburnean basement during OG genesis. This result aligns with significant inherited Paleoproterozoic zircon populations reported for OG rocks across the Anti-Atlas. For instance, Baidada et al. (2019) reported a Paleoproterozoic signature in Saghro massif granitoids, while Blein et al. (2014b) and Thomas et al. (2002) documented similar inheritance in OG ignimbrites from the Agadir Melloul area and syn-extensional granites in the Sirwa massif, respectively.

5.5 Further discussions

At a regional scale, basaltic flows have been described as interbedded within the SG sediments of the Saghro massif (Errami et al., 2009; Fekkak et al., 2003, 2001). These flows exhibit diverse geochemical signatures. The basalts in Sidi Flah (SF) are of Initial Rift Tholeiites (IRT) and Ocean Island Basalts (OIB) character (Fekkak et al., 2001). In contrast, the Anou N'Izem basalts in the Boumalne (BO) inlier possess typical Mid-Ocean Ridge Basalt (MORB) signatures (Errami et al., 2009). U-Pb dating of detrital zircons from the SG in various inliers suggests this unit was deposited between 640–600 Ma across the entire Central-Eastern Anti-Atlas region (Errami et al., 2021a; Abati et al., 2010).

In liaison, this geochemical variation within the SG likely reflects a single, continuous geodynamic event. Specifically, during the evolution of a back-arc basin, the earliest magmas often exhibit magmatic arc-like characteristics due to the proximity of the back-arc to the arc itself; as the back-arc matures and the magma source becomes further removed from the metasomatized mantle, magmas transition toward within-plate (OIB) and MORB-like signatures (Vasey et al., 2021; Saunders and Tarney, 1984). This interpretation is further supported by sediment geochemistry pointing toward a back-arc basin depositional environment (Ouguir et al., 1996). In the Anti-Atlas, this footprint is widely attributed to activation of a sub continental lithospheric mantle source, previously metasomatized during earlier Cryogenian Pan-African subduction, operating in tandem with distal stress fields from the emerging Cadomian orogenic system (Hefferan et al., 2014). As the basin matured and lithospheric extension advanced, the magma source increasingly tapped deeper, uncontaminated asthenospheric reservoirs, driving a compositional transition toward within-plate (OIB) and MORB-like signatures higher up the stratigraphy. Basaltic magmatism in the SG fits this evolutionary framework: the calc-alkaline basalts from the Sirwa inlier (Thomas et al., 2002; this study) represent the initial stages of back-arc formation, recording activation of this strongly metasomatized mantle source, whereas the IRT, OIB, and MORB-type basalts found higher in the stratigraphy indicate a more mature, extensional stage tapping deeper, uncontaminated asthenospheric reservoirs.

The thick volcano-sedimentary successions of the OG are dominated by silicic to intermediate high-K calc-alkaline to shoshonitic volcanism (Blein et al., 2014b; Toummite et al., 2013; Walsh et al., 2012; Gasquet et al., 2008, 2005; Benziane, 2007; Thomas et al., 2004; El Baghdadi et al., 2003). Based on our findings, and regional correlations with similar magmatism (see Table 1 in Hefferan et al. (2014), for reported precise ages from selected Anti-Atlas inliers), we attribute the OG rocks to a widespread post-collisional event, recognized across numerous inliers of the Anti-Atlas (Yajioui et al., 2020; Karaoui et al., 2015; Linnemann et al., 2014; Toummite et al., 2013; Walsh et al., 2012; Gasquet et al., 2005, 2004; Thomas et al., 2002). For the studied OG rocks, high Th/Nb ratios suggest that slab break-off induced a thermal pulse supplying heat to melt the Lower Continental Crust (LCC), with variable input from a metasomatized mantle wedge previously primed during an earlier subduction phase. Clustering near and above the Upper Continental Crust (UCC) field further indicates that lithospheric delamination supplied the necessary thermal energy to trigger widespread crustal melting, producing the high-K and shoshonitic signatures of the OG rocks (Bonin, 2004). This magmatism was coeval with a Silicic Large Igneous Province (SLIP) recognized across the Anti-Atlas (Ousbih et al., 2024, and references therein; Schulte et al., 2022).

6 Conclusions

In the light of the above, the following conclusions can be drawn:

i. LA-ICP-MS U-Pb zircon ages of 575 ± 3 Ma and 564 ± 2 Ma from the OG reflect post-collisional, syn-orogenic magmatism in the ZGMR, spanning roughly 11 million years. Detrital zircons from the SG reveal a single-population at ca. 2100 Ma and a MDA of 2025 Ma, with no younger Neoproterozoic/Pan-African grains, demonstrating exclusive sediment derivation from an adjacent, uplifted pristine block of Eburnean basement and supporting northward extension of the WAC beyond the AAMF.

ii. Based on geochemical proxies (major and trace elements). The SG magmatic rocks were emplaced during early back-arc basin opening, as indicated by their calc-alkaline affinity, geochemical characteristics, and regional correlations. Their εNd_{620} values (+3.2 and +4.6) and TDM ages (1.02 and 0.91 Ga) reflect a mixed mantle-crustal origin, combining mostly mantle-derived magma with limited contribution from older crustal material consistent with an underlying Paleoproterozoic to Mesoproterozoic crust.

iii. The OG high-K calc-alkaline to shoshonitic suite evolved mainly through fractional crystallization and crustal contamination. They were deposited in a post-collisional setting and sourced from an enriched continental lithospheric mantle, previously underwent metasomatism by fluids from former Neoproterozoic subduction. Their εNd_{570} values (-0.8 to +1.1) and TDM ages (1.30 to 1.15 Ga) imply significant reworking of older, evolved Paleoproterozoic continental crustal during Ediacaran times.

iv. The OG rocks of the ZGMR record lithospheric delamination and potential slab break-off driving post-collisional petrogenesis, linked to the late Neoproterozoic SLIP along the northwestern edge of the WAC.

Code, data, or code and data availability

Data used in this paper is given in electronic supplements.

Supplement link

Author contributions

Abdelhay Ben-Tami: Field work, Sampling and preparation, Thin-sections preparation, Investigation, Data visualization, Data curation, Formal analysis, Writing of original draft, Finalization. **Said Belkacim:** Supervision, Resources, Writing - review and editing. **Jamal El Kabouri:** Data visualization, Writing of original draft. Review and editing. **Joshua H.F.L. Davies and Morgann G. Perrot:** LA-ICP-MS U-Pb data and methodology, writing of original draft, review and editing. **Mariam Ferraq**: Data curation and visualization. **Mohamed Bouabdellah:** review and editing. **Bouchra Baidada, Mohamed Bhilisse** and **Mohamed Assalmi:** Resources, accommodation, field trips, hosting.

Competing interests

The authors declare that they have no conflict of interest. Corresponding author (Abdelhay Ben-Tami), discloses an employment relationship with the Zgounder Millenium Silver Mining Company (ZMSM).

Disclaimer

Copernicus Publications remains neutral with regard to jurisdictional claims made in the text, published maps, institutional affiliations, or any other geographical representation in this paper. While Copernicus Publications makes every effort to include appropriate place names, the final responsibility lies with the authors. Views expressed in the text are those of the authors and do not necessarily reflect the views of the publisher.

Acknowledgements

This research represents a component of the corresponding author's thesis project. The authors express their sincere gratitude to the **Zgounder Millenium Silver Mining Company (ZMSM)**, the Moroccan subsidiary of **Aya Gold and Silver (AYA)**, for their essential financial support for this study, as well as for providing accommodation and logistical assistance. Special appreciation is extended to the Exploration geology team at the Zgounder Mine for their valuable facilitation and support during field operations. Official permission to publish this work was granted by **David Lalonde, P. Geo / VP Exploration / Aya Gold and Silver Inc.**

Financial support

Financial support for Whole-rock analysis, Sm-Nd isotopes, U-Pb on zircon, fieldwork and accommodation was guaranteed by the **Zgounder Millenium Silver Mining company (ZMSM)**.

Review statement

References

Abati, J., Aghzer, A. M., Gerdes, A., & Ennih, N.: Detrital zircon ages of Neoproterozoic sequences of the Moroccan Anti-Atlas belt. Precambrian Research, 181(1-4), 115–128, https://doi:10.1016/j.precamres.2010.05.018, 2010.

Admou, H., Fekkak, A., Razin, P., Egal, E., Youbi, N., Soulaimani, A., Blein, O., Baudin, T., Chevremont, P.: Carte géologique Maroc (1/50 000), feuille d'Aït Ahmane– Notes et Mémoires Service Géologique Maroc, no. 533, 2012.

Aït Malek, A., Gasquet, D., Bertrand, J.M., Leterrier, J. : Géochronologie U-Pb sur zircon de granitoïdes éburnéens et panafricains dans les boutonnières protérozoïques d'Igherm, du Kerdous et du Bas Drâa (Anti-Atlas occidental, Maroc). Comptes. Rendus. l'Académie des Sciences-Series. IIA–Earth and Planetary Science. 327 (12), 819–826, https://doi.org/10.1016/S1251-8050(99)80056-1, 1998.

Álvaro, J.J., Benziane, F., Thomas, R., Walsh, G.J., Yazidi, A.: Neoproterozoic–Cambrian stratigraphic framework of the Anti–Atlas and Ouzellagh promontory (High Atlas), Morocco. Journal of African Earth Sciences. 98, 19–33, https://doi.org/10.1016/j.jafrearsci.2014.04.026, 2014.

Álvaro, J. J., Pouclet, A., Ezzouhairi, H., Soulaimani, A., Bouougri, E. H., Imaz, A. G., and Fekkak, A.: Early Neoproterozoic rift-related magmatism in the Anti-Atlas margin of the West African craton, Morocco. Precambrian Research, 255, 433-442, https://doi.org/10.1016/j.precamres.2014.10.008, 2014b.

Baidada, B., Ikenne, M., Barbey, P., Soulaimani, A., Cousens, B., Haissen, F., Ilmen, Said, Alansari, A.: SHRIMP U–Pb zircon geochronology of the granitoids of the Imiter Inlier: constraints on the Pan-African events in the Saghro massif, Anti-Atlas (Morocco). Journal of African Earth Sciences. 150, 799–810, https://doi.org/10.1016/j. jafrearsci.2018.10.008, 2019.

Bajja, A.: Volcanisme syn à post orogénique du Néoprotérozoïque de l'Anti-Atlas: implications pétrogénétiques et géodynamiques. In: de Wall H., Greiling R.P. (Eds.), Magmatic Evolution of a Neoproterozoic Island-Arc Syn- to Postorogenic Igneous Activity in the Anti-Atlas (Morocco). Forschunszentrum Jülich Gmbh 45, pp. 9–228, 2001.

Ben-Tami, A., Belkacim, S., Baidada, B., El Kabouri, J., Assalmi, M., Bhilisse, M., and Bouabdellah, M.: Lithostratigraphy, Whole-Rock, and Sm–Nd Isotopic Data of the Ediacaran Magmatic Rocks from the Zgounder Ag–Hg Deposit (Siroua Massif, Central Anti-Atlas, Morocco). In international conference on Mediterranean Geosciences Union (pp. 167-171). Cham: Springer Nature Switzerland, https://doi.org/10.1007/978-3-031-48758-3_38, 2024.

Benziane, F.: Lithostratigraphie et évolution géodynamique de l'Anti-Atlas (Maroc) du Paléoprotérozoïque au Néoprotérozoïque: exemples de la boutonnière de Tagragra de Tata et du Jbel Saghro. Thèse de doctorat, Université de Savoie CISM, Chambéry, France. 321 pp, 2007.

Blein, O., Baudin, T., Chevremont, P., Gasquet, D.: Petrogenesis of late Ediacaran volcanic rocks of the Kerdous and Tagragra d'Akka inliers (Anti-Atlas Morocco): involvement of slab-failure. Journal of African Earth Sciences, 199, 104831, https://doi.org/10.1016/j.jafrearsci.2023.104831, 2023.

Blein, O., Baudin, T., Chèvremont, P., Soulaimani, A., Admou, H., Gasquet, P., … Gombert, P.: Geochronological constraints on the polycyclic magmatism in the Bou Azzer-El Graara inlier (Central Anti-Atlas Morocco). Journal of African Earth Sciences, 99, 287–306, https://doi:10.1016/j.jafrearsci.2014.04.021, 2014.

Blein, O., Baudin, T., Soulaimani, A., Cocherie, A., Chèvremont, P., Admou, H., … Roger, J.: New geochemical, geochronological and structural constraints on the Ediacaran evolution of the south Sirwa, Agadir-Melloul and Iguerda inliers, Anti-Atlas, Morocco. Journal of African Earth Sciences, 98, 47–71, https://doi:10.1016/j.jafrearsci.2014.06.019, 2014b.

Bonin, B.: Do coeval mafic and felsic magmas in post-collisional to within-plate regimes necessarily imply two contrasting, mantle and crustal, sources? A review. Lithos, 78(1-2), 1-24, https://doi.org/10.1016/j.lithos.2004.04.042, 2004.

Boynton, W. V.: Cosmochemistry of the rare earth elements: meteorite studies. In Developments in geochemistry, Elsevier, (Vol. 2), (pp. 63-114), https://doi.org/10.1016/B978-0-444-42148-7.50008-3, 1984.

Cabanis B, Lecolle M.: Le diagramme La/10–Y/15–Nb/8: un outil pour la discrimination des séries volcaniques et la mise en évidence des processus de mélange et/ou de contamination crustale. Comptes Rendus de l'Académie des Sciences, Paris, Série II 309:2023–2029, 1989.

Choubert, G.: Essai de mise au point du problème des "ignimbrites". Bulletin Volcanologique, 25(1), 123-140, https://doi.org/10.1007/BF02596545, 1963.

De Beer, C.H., Chevallier, L.P., De Kock, G.S., Gresse, P.G., Thomas, R.J.: Notice Explicative de la Carte Géologique du Maroc au 1/50 000 feuille Sirwa. Notes et Mémoires Service Géologique. Maroc 395, 86, 2000.

Dickinson, W.R., Gehrels, G.E.: Use of U–Pb ages of detrital zircons to infer maximum depositional ages of strata: a test against a Colorado Plateau Mesozoic database. Earth and Planetary Science Letters. 288, 115–125, https://doi.org/10.1016/j.epsl.2009.09.013, 2009.

D'Lemos, R. S., Inglis, J. D., and Samson, S. D.: A newly discovered orogenic event in Morocco: Neoproterozoic ages for supposed Eburnean basement of the Bou Azzer inlier, Anti-Atlas Mountains. Precambrian Research, 147(1-2), 65–78, https://doi:10.1016/j.precamres.2006.02.003, 2006.

Eby, G. N.: Chemical subdivision of the A-type granitoids: petrogenetic and tectonic implications. Geology, 20(7), 641-644, https://doi.org/10.1130/0091-7613(1992)020<0641:CSOTAT>2.3.CO;2, 1992.

El Baghdadi, M., El Boukhari, A., Jouider, A., Benyoucef, A., Nadem, S.: Calc-alkaline arc I-type granitoid associated with S-type granite in the Pan-African belt of eastern Anti-Atlas (Saghro and Ougnat, South Morocco). Gondwana Research. 6 (4), 557–572, https://doi.org/10.1016/S1342-937X(05)71007-8, 2003.

El Hadi, H., Simancas, J.F., Martínez-Poyatos, D., Azor, A., Tahiri, A., Montero, P., Fanning, C.M., Bea, F., Gonzalez-Lodeiro, F.: Structural and geochronological constraints on the evolution of the Bou Azzer Neoproterozoic ophiolite (Anti-Atlas, Morocco). Precambrian Research. 182 (1–2), 1–14, https://doi.org/10.1016/j. precamres.2010.06.011, 2010.

Ennih, N., and Liégeois, J. P.: The boundaries of the West African craton, with special reference to the basement of the Moroccan metacratonic Anti-Atlas belt. Geological Society, London, Special Publications, 297(1), 1–17, https://doi.org/10.1144/SP297.1, 2008.

Ennih, N., and Liégeois, J.P.: The Moroccan Anti-Atlas: the West African craton passive margin with limited Pan-African activity. Implications for the northern limit of the craton. Precambrian Research. 112 (3–4), 289–302, https://doi.org/10.1016/S0301-9268 (01)00195-4, 2001.

Errami, E., Linnemann, U., Hofmann, M., G¨artner, A., Zieger, J., G¨artner, J., Mende, K., El Kabouri, J., Gasquet, D., Ennih, N.: From Pan-African transpression to Cadomian transtension at the west African margin: New U-Pb zircon ages from the eastern saghro inlier (anti-atlas, Morocco). Geological Society. Special Publications. 503, 209–233, https://doi.org/10.1144/SP503-2020-105, 2021a.

Errami, E., Bonin, B., Laduron, D., Lasri, L.: Petrology and geodynamic significance of the post-collisional Pan-African magmatism in the Eastern Saghro area (Anti- Atlas, Morocco). Journal of African Earth Sciences. 55 (1–2), 105–124, https://doi.org/10.1016/j. jafrearsci.2009.02.006, 2009.

Faure, G.: Isotope systematics in two-component mixtures. Principles of isotope geology, 2 edn. John Wiley & Sons, Chichester, 141-153, 1986.

Fekkak, A., Pouclet, A., & Benharref, M.: The middle Neoproterozoic sidi flah group (Anti-Atlas, Morocco): syn-rift deposition in a Pan-African continent/ocean transition zone. Journal of African Earth Sciences, 37(1-2), 73-87, https://doi.org/10.1016/S0899-5362(03)00049-6, 2003.

Fekkak, A., Pouclet, A., & Badra, L.: The pre-Pan-African rifting of Saghro (Anti-Atlas, Morocco): example of the middle Neoproterozoic basin of Boumalne. Bulletin de la Société géologique de France, 173(1), 25-35, https://doi.org/10.2113/173.1.25, 2002.

Fekkak, A., Pouclet, A., Ouguir, H., Ouazzani, H., Badra, L., Gasquet, D.: Géochimie et signification géotectonique des volcanites du Cryogénien inférieur du Saghro (Anti-Atlas oriental, Maroc) /Geochemistry and geotectonic significance of Early Cryogenian volcanics of Saghro (Eastern Anti-Atlas, Morocco). Geodinamica. Acta, 14 (6), 373–385, https://doi.org/10.1080/09853111.2001.10510730, 2001.

Ferraq, M., Belkacim, S., Cheng, L. Z., Davies, J. H., Perrot, M. G., Ben-Tami, A., & Bouabdellah, M.: New Geochemical and Geochronological Constraints on the Genesis of the Imourkhssen Cu±Mo±Au±Ag Porphyry Deposit (Ouzellagh-Siroua Salient, Anti-Atlas, Morocco): Geodynamic and Metallogenic Implications. Minerals, 14(8), 832, https://doi.org/10.3390/min14080832, 2024.

Gasquet, D., Ennih, N., Liégeois, J.P., Soulaimani, A., Michard, A.: The Pan-African Belt. In: Michard, A., Saddiqi, O., Chalouan, A., Frizon de Lamotte, D. (Eds.), Continental evolution: the geology of Morocco. Lect. Notes Earth Sci. 116, 33–64, https://doi.org/10.1007/978-3-540-77076-3_2, 2008.

Gasquet, D., Levresse, G., Cheilletz, A., Azizi-Samir, M. R., and Mouttaqi, A.: Contribution to a geodynamic reconstruction of the Anti-Atlas (Morocco) during Pan-African times with the emphasis on inversion tectonics and metallogenic activity at the Precambrian–Cambrian transition. Precambrian Research, 140(3-4), 157–182, https://doi:10.1016/j.precamres.2005.06.009, 2005.

Gasquet, D., Chevremont, P., Baudin, T., Chalot-Prat, F., Guerrot, C., Cocherie, A., and Cheilletz, A.: Polycyclic magmatism in the tagragra d’akka and kerdous–tafeltast inliers (western Anti-Atlas, Morocco). Journal of African Earth Sciences, 39(3-5), 267-275, https://doi.org/10.1016/j.jafrearsci.2004.07.062, 2004.

Goldstein, S. L., O'nions, R. K., and Hamilton, P. J.: A Sm-Nd isotopic study of atmospheric dusts and particulates from major river systems. Earth and planetary Science letters, 70(2), 221-236, https://doi.org/10.1016/0012-821X(84)90007-4, 1984.

Green, T. H.: Significance of Nb/Ta as an indicator of geochemical processes in the crust-mantle system. Chemical geology, 120(3-4), 347-359, https://doi.org/10.1016/0009-2541(94)00145-X, 1995.

Gresse, P.G., De Beer, C.H., Chevallier, L.P., De Kock, G.S., Thomas, R.J. : Notice Explicative de la Carte Géologique du Maroc au 1/50 000 feuille Tachoukacht. Notes et Mémoires Service Géologique. Maroc 393, 106, 2000.

Hastie, A.R., Kerr, A.C., Pearce, J.A., Mitchell, S.F.: Classification of altered volcanic island arc rocks using immobile trace elements: development of the Th–Co discrimination diagram. Journal of Petrology. 48 (12), 2341–2357, https://doi.org/10.1093/ petrology/egm062, 2007.

Hefferan, K., Soulaimani, A., Samson, S. D., Admou, H., Inglis, J., Saquaque, A., … Heywood, N.: A reconsideration of Pan African orogenic cycle in the Anti-Atlas Mountains, Morocco. Journal of African Earth Sciences, 98, 34–46, https:// doi:10.1016/j.jafrearsci.2014.03.007, 2014.

Hofmann, A. W., Jochum, K. P., Seufert, M., & White, W. M.: Nb and Pb in oceanic basalts: new constraints on mantle evolution. Earth and Planetary science letters, 79(1-2), 33-45, https://doi.org/10.1016/0012-821X(86)90038-5, 1986.

Horstwood, M. S., Košler, J., Gehrels, G., Jackson, S. E., McLean, N. M., Paton, C., ... and Schoene, B.: Community-derived standards for LA-ICP-MS U-(Th-) Pb geochronology–Uncertainty propagation, age interpretation and data reporting. Geostandards and Geoanalytical Research, 40(3), 311-332, https://doi.org/10.1111/j.1751-908X.2016.00379.x, 2016.

Hughes, C. J.: Spilites, keratophyres, and the igneous spectrum. Geological Magazine, 109(6), 513-527, https://doi.org/10.1017/S0016756800042795, 1972.

Ikenne, M., Ennaciri, A., Ouguir, H., Cousens, B., Ziyadi, R., Mouhagir, M., & El-Gaouzi, A.: Geochemical Signature And Geodynamic Significance Of An Ag-Hg Mineralized Dyke Swarm In The Neoproterozoic Inlier Of Imiter - Anti-Atlas (Morocco). Ofioliti, 32(2), 109–118, https://doi.org/10.4454/ofioliti.v32i2.351, 2007.

Janoušek, V., Farrow, C. M., & Erban, V.: Interpretation of whole-rock geochemical data in igneous geochemistry: introducing Geochemical Data Toolkit (GCDkit). Journal of Petrology, 47(6), 1255-1259, https://doi.org/10.1093/petrology/egl013, 2006.

Janoušek, V., Moyen, J. F., Martin, H., Erban, V., & Farrow, C.: Geochemical modelling of igneous processes: principles and recipes in R language. Bringing the Power of R to a Geochemical Community. Springer, Berlin, https://doi.org/10.1007/978-3-662-46792-3, 2016.

Karaoui, B., Breitkreuz, C., Mahmoudi, A., Youbi, N., Hofmann, M., Gärtner, A., & Linnemann, U.: U–Pb zircon ages from volcanic and sedimentary rocks of the Ediacaran Bas Draâ inlier (Anti-Atlas Morocco): Chronostratigraphic and provenance implications. Precambrian Research. 263, 43–58, https://doi:10.1016/j.precamres.2015.03.003, 2015.

Labanieh, S.; Chauvel, C.; Germa, A.; Quidelleur, X.: Martinique: a Clear Case for Sediment Melting and Slab Dehydration as a Function of Distance to the Trench. Journal of Petrology, 53(12), 2441–2464. https://doi:10.1093/petrology/egs055, 2012.

Leblanc, M., & Lancelot, J. R.: Interprétation géodynamique du domaine pan-africain (Précambrien terminal) de l’Anti-Atlas (Maroc) à partir de données géologiques et géochronologiques. Canadian Journal of Earth Sciences, 17(1), 142–155, https://doi:10.1139/e80-012, 1980.

Letsch, D., Houicha, M. E., von Quadt, A., and Winkler, W.: missing link in the peri-Gondwanan terrane collage: the Precambrian basement of the Moroccan Meseta and its lower Paleozoic cover. Canadian Journal of earth sciences, 55(1), 33-51, https://doi.org/10.1139/cjes-2017-0086, 2018.

Liégeois, J.P., Abdelsalam, M.G., Ennih, N., Ouabadi, A.: Metacraton: nature, genesis and behavior. Gondwana Res. 23 (1), 220–237, https://doi.org/10.1016/j. gr.2012.02.016, 2013.

Liégeois, J.P., Fekkak, A., Bruguier, O., Errami, E., Ennih, N.: The Lower Ediacaran (630–610 Ma) Saghro group: an orogenic transgressive basin development during the early metacratonic evolution of the Anti-Atlas (Morocco). In: IGCP485 4th meeting, Algiers, p. 57, 2006.

Liew, T. C., & Hofmann, A. W.: Precambrian crustal components, plutonic associations, plate environment of the Hercynian Fold Belt of central Europe: indications from a Nd and Sr isotopic study. Contributions to Mineralogy and Petrology, 98(2), 129-138, https://doi.org/10.1007/BF00402106, 1988.

Linnemann, U., Gerdes, A., Hofmann, M., Marko, L.: The Cadomian Orogen: Neoproterozoic to Early Cambrian crustal growth and orogenic zoning along the periphery of the West African Craton-Constraints from U-Pb zircon ages and Hf isotopes (Schwarzburg Antiform, Germany). Precambrian Research. 244, 236–278, https://doi.org/10.1016/j.precamres.2013.08.007, 2014.

Linnemann, U., Pereira, F., Jeffries, T.E., Drost, K., Gerdes, A.: The Cadomian Orogeny and the opening of the Rheic Ocean: the diacrony of geotectonic processes constrained by LA-ICP-MS U–Pb zircon dating (Ossa-Morena and Saxo-Thuringian Zones, Iberian and Bohemian Massifs). Tectonophysics 461, 21–43, https://doi.org/ 10.1016/j.tecto.2008.05.002, 2008.

Michard, A., Soulaimani, A., Ouanaimi, H., Raddi, Y., Brahim, L.A., Rjimati, E.C., Saddiqi, O.: Saghro Group in the Ougnat Massif (Morocco), an evidence for a continuous Cadomian basin along the northern West African Craton. Comptes Rendus Géosciences. 349 (2), 81–90, https://doi.org/10.1016/j.crte.2017.01.001, 2017.

Middlemost, E. A.: Naming materials in the magma/igneous rock system. Earth-science reviews, 37(3-4), 215-224, https://doi.org/10.1016/0012-8252(94)90029-9, 1994.

Mrini, Z.: Chronologie (Rb-Sr, U-Pb), traçage isotopique (Sr-Nd-Pb) des sources de roches magmatiques éburnéenne, panafricaine et hercynienne du Maroc. Un-published thesis. University of Marrakech, Morocco, 200 p, 1993.

Nance, R. D., Murphy, J. B., Strachan, R. A., Keppie, J. D., Gutiérrez-Alonso, G., Fernández-Suárez, J., ... & Pisarevsky, S. A.: Neoproterozoic–early Palaeozoic tectonostratigraphy and palaeogeography of the peri-Gondwanan terranes: Amazonian v. West African connections. Geological Society, London, Special Publications, 297, 345–383, https://doi.org/10.1144/SP297.17, 2008.

O’Connor, E.A., Barnes, R.P., Beddoe-Stephens, B., Fletcher, T., Gillespie, M.R., Hawkins, M.P., Loughlin, S.C., Smith, M., Smith, R.A., Waters, C.N., Williams, M.: Geology of the Drâa, Kerdous, and Boumalne Districts, Anti-Atlas. Keyworth, Nottingham British Geological Survey, Morocco, p. 324, 2010.

Ouabid, M., Garrido, C.J.: Widespread Cadomian–Pan-African Ediacaran magmatism across the Moroccan Meseta: implication for the geodynamic evolution of the NW Gondwana margin. Precambrian Research. 387, https://doi.org/10.1016/j.precamres.2023.106992, 2023.

Ougadire, M., Askkour, F., Favier, A., Ousbih, M., Ikenne, M., & Géraud, Y.: Petrogenesis of the late Ediacaran A-type granites of the western part of the Moroccan Anti-Atlas belt: Insights from U–Pb dating, geochemistry and Sr–Nd isotopes of the Sidi El Houssein, Tafraout and Taourgha intrusions. Journal of African Earth Sciences, 203, 104947, https://doi.org/10.1016/j.jafrearsci.2023.104947, 2023.

Ouguir, H., Macaudière, J., Dagallier, G. : Le Protérozoïque supérieur d'Imiter, Saghro oriental, Maroc : un contexte géodynamique d'arrière-arc. Journal of African Earth Sciences. 22 (2), 173–189, https://doi.org/10.1016/0899-5362(96)00002-4, 1996.

Ousbih, M., Ikenne, M., Cousens, B., Chelle-Michou, C., El Bilali, H., Gaouzi, A., ... & Ernst, R.: Stratigraphy, geochronology, geochemistry and Nd isotopes of the Ouarzazate Group, Anti-Atlas, Morocco: Evidence of a Late Neoproterozoic LIP in the northwestern part of the West African Craton. Lithos, 474, 107593., https://doi.org/10.1016/j.lithos.2024.107593, 2024.

Pearce JA, Ernst RE, Peate DW, Rogers C.: LIP printing: use of immobile element proxies to characterize Large Igneous Provinces in the geologic record. Lithos 392–393:106068, https://doi.org/10.1016/j.lithos.2021.106068, 2021.

Pearce, J. A.: Geochemical fingerprinting of oceanic basalts with applications to ophiolite classification and the search for Archean oceanic crust. Lithos, 100(1-4), 14-48, https://doi.org/10.1016/j.lithos.2007.06.016, 2008.

Pelleter, E., Cheilletz, A., Gasquet, D., Mouttaqi, A., Annich, M., Camus, Q., Deloule, E., Ouazzani, L., Bounajma, H., Ouchtouban, L.: U/Pb ages of magmatism in the Zgounder Epithermal Ag–Hg Deposit, Sirwa Window, Anti-Atlas, Morocco. In: Mineral Deposits of North Africa. Springer, pp. 143–165, https://doi.org/10.1007/978-3-319-31733-5_5, 2016.

Pereira, M. F., El Houicha, M., Chichorro, M., Armstrong, R., Jouhari, A., El Attari, A., and Silva, J. B.: Evidence of a Paleoproterozoic basement in the Moroccan Variscan belt (Rehamna massif, western Meseta). Precambrian Research, 268, 61-73, https://doi.org/10.1016/j.precamres.2015.07.010, 2015.

Rojo-Pérez, E., Arenas, R., Fuenlabrada, J. M., Novo-Fernández, I., Martínez, S. S., Moreno-Martín, D., and Fernández, R. D.: Lower Cambrian magmatism in the SW Iberian sector of the African–Gondwana margin: geochemical and isotopic keys to incipient tectonic switching, https://doi.org/10.1144/SP542-2022-294, 2024.

Saadi, A.: Contribution à l'étude écologique de deux hydrosystèmes temporaires saumâtres du Maroc : Zima et Sedd-El-Messjoun (Bassin de la Bahira). PhD thesis, Semlalia Faculty, University of Cady Ayyad, Marrakech, Morocco, 1985.

Samson, S. D., Inglis, J. D., D'Lemos, R. S., Admou, H., Blichert-Toft, J., and Hefferan, K.: Geochronological, geochemical, and Nd–Hf isotopic constraints on the origin of Neoproterozoic plagiogranites in the Tasriwine ophiolite, Anti-Atlas orogen, Morocco. Precambrian Research, 135(1-2), 133–147, https://doi:10.1016/j.precamres.2004.08.003, 2004.

Saunders, A. D., and Tarney, J.: Geochemical characteristics of basaltic volcanism within back-arc basins. Geological Society, London, Special Publications, 16(1), 59-76, https://doi.org/10.1144/GSL.SP.1984.016.01.05, 1984.

Schulte, B., Boger, S.D., Benziane, F., Yazidi, A., Fanning, C.M.: The Ouarzazate Supergroup and its plutonic keel: the relics of an Ediacaran silicic large igneous province in North Africa. Journal of the Geological Society. London. 179, 5, https://doi.org/10.1144/ jgs2021-114, 2022.

Shand, S. J.: Eruptive rocks; their genesis, composition, classification, and their relation to ore-deposits with a chapter on meteorite. New York: John Wiley & Sons, 1943.

Shervais, J. W.: The petrogenesis of modern and ophiolitic lavas reconsidered: Ti-V and Nb-Th. Geoscience Frontiers, 13(2), 101319, https://doi.org/10.1016/j.gsf.2021.101319, 2022.

Soulaimani, A., Ouanaimi, H., Saddiqi, O., Baidder, L., and Michard, A.: The Anti-Atlas Pan-African Belt (Morocco): Overview and pending questions. Comptes Rendus Géoscience, https://doi:10.1016/j.crte.2018.07.002, 2018.

Stern, R. J.: A reinterpretation of the past 2.5 billion years of Earth's tectonic history: Two episodes each of plate and single-lid tectonics. Geological Society of America Bulletin, https://doi.org/10.1130/B37966.1, 2024.

Sun, S. S., and McDonough, W. F.: Chemical and isotopic systematics of oceanic basalts: implications for mantle composition and processes. Geological Society, London, Special Publications, 42(1), (pp. 313-345), https://doi.org/10.1144/GSL.SP.1989.042.01.19, 1989.

Tahiri, A., Montero, P., El Hadi, H., Poyatos, D. M., Azor, A., Bea, F., and Lodeiro, F. G.: Geochronological data on the Rabat–Tiflet granitoids: their bearing on the tectonics of the Moroccan Variscides. Journal of African Earth Sciences, 57(1-2), 1-13, https://doi.org/10.1016/j.jafrearsci.2009.07.005, 2010.

Thomas, R. J., Fekkak, A., Ennih, N., Errami, E., Loughlin, S. C., Gresse, P. G., Liégeois, J.-P.: A new lithostratigraphic framework for the Anti-Atlas Orogen, Morocco. Journal of African Earth Sciences, 39(3-5), 217–226, https://doi:10.1016/j.jafrearsci.2004.07.046, 2004.

Thomas, R. ., Chevallier, L. ., Gresse, P. ., Harmer, R. ., Eglington, B. ., Armstrong, R. ., Ingram, B.: Precambrian evolution of the Sirwa Window, Anti-Atlas Orogen, Morocco. Precambrian Research, 118(1-2), 1–57, https://doi:10.1016/s0301-9268(02)00075-x, 2002.

Thomas, R.J., De Beer, C.H., Chevallier, L.P., De Kock, G.S., Gresse, P.G.: Notice Explicative de la Carte Géologique du Maroc au 1/50 000 feuille Assarag. Notes et Mémoires Service Géologique. Maroc 392, 84, 2000a.

Toummite, A., Liégeois, J.P., Gasquet, D., Bruguier, O., Beraaouz, E.H., Ikenne, M.: Field, geochemistry and Sr-Nd isotopes of the Pan-African granitoids from the Tifnoute Valley (Sirwa, Anti-Atlas, Morocco): a post-collisional event in a metacratonic setting. Mineralogy and Petrology. 107 (5), 739–763, https://doi.org/10.1007/ s00710-012-0245-3, 2013.

Vasey, D. A., Cowgill, E., & Cooper, K. M.: A preliminary framework for magmatism in modern continental back-arc basins and its application to the Triassic-Jurassic tectonic evolution of the Caucasus. Geochemistry, Geophysics, Geosystems, 22(6), e2020GC009490, https://doi.org/10.1029/2020GC009490, 2021.

Vermeesch, P.: IsoplotR: A Free and Open Toolbox for Geochronology. Geoscience Frontiers. 9 (5), 1479–1493, https://doi.org/10.1016/j.gsf.2018.04.001, 2018.

Vermeesch, P.: How many grains are needed for a provenance study?. Earth and Planetary Science Letters, 224(3-4), 441-451, https://doi.org/10.1016/j.epsl.2004.05.037, 2004.

Walsh, G.J., Aleinikoff, J.N., Harrison, R.W., Yazidi, A., Burton, W.C., Quick, J.E., Benziane, F., Yazidi, A., Saadane, A.: Neoproterozoic tectonic evolution of the Jebel Saghro and Bou Azzer—El Graara inliers, eastern and central Anti-Atlas, Morocco. Precambrian Research. 216, 23–62, https://doi.org/10.1016/j. precamres.2012.06.010, 2012.

Walsh, G. J., Aleinikoff, J. N., Benziane, F., Yazidi, A., & Armstrong, T. R.: U–Pb zircon geochronology of the Paleoproterozoic Tagragra de Tata inlier and its Neoproterozoic cover, western Anti-Atlas, Morocco. Precambrian Research, 117(1-2), 1-20, https://doi.org/10.1016/S0301-9268(02)00044-X, 2002.

Wilson, M. (Ed.).: Igneous petrogenesis. Dordrecht: Springer Netherlands, 1989.

Winchester, J. A., and Floyd, P. A.: Geochemical discrimination of different magma series and their differentiation products using immobile elements. Chemical geology, 20, (pp. 325-343), https://doi.org/10.1016/0009-2541(77)90057-2, 1977.

Yajioui, Z., Karaoui, B., Chew, D., Breitkreuz, C., Mahmoudi, A.: U–Pb zircon geochronology of the Ediacaran volcano-sedimentary succession of the NE Saghro inlier (Anti-Atlas, Morocco): chronostratigraphic correlation on the northwestern margin of Gondwana. Gondwana Research. 87, 263–277, https://doi.org/10.1016/j. gr.2020.06.015, 2020.

Youbi, N., Ernst, R.E., Soderlund, U., Boumehdi, M.A., Ait Lahna, A., Tassinari, C.C.G., El Moume, W., Bensalah, M.K.: The Central Iapetus magmatic province: an updated review and link with the ca. 580 Ma Gaskiers glaciation. In: Adatte, T., Bond, D.P.G., Keller, G. (Eds.), Mass Extinctions, Volcanism, and Impacts: New Developments: Geological Society of America Special Paper, 544, pp. 35–66, https://doi.org/10.1130/2020.2544(02), 2020.